Andean Geology
ISSN: 0718-7092
revgeologica@sernageomin.cl
Servicio Nacional de Geología y Minería
Chile

Calderón, Mauricio; Hervé, Francisco; Cordani, Umberto; Massonne, Hans-Joachim
Crust-mantle interactions and generation of silicic melts: insights from the Sarmiento Complex, southern Patagonian Andes
Andean Geology, vol. 34, núm. 2, julio, 2007, pp. 249-275
Servicio Nacional de Geología y Minería
Santiago, Chile

Crust-mantle interactions and generation of silicic melts: insights from the Sarmiento Complex, southern Patagonian Andes

Mauricio Calderón
Francisco Hervé

Departamento de Geología, Universidad de Chile,
Casilla 13518, Correo 21,Santiago, Chile
caldera@esfera.cl
fherve@cec.uchile.cl

Umberto Cordani

Centro de Pesquisas Geocronológicas, Universidade de São Paulo,
Rua do Lago 562, Cidade Universitaria, São Paulo, CEP 05508-900, Brazil
ucordani@usp.br

Hans-Joachim Massonne

Institut für Mineralogie und Kristallchemie, Universität Stuttgart,
Azenbergstrasse 18, D-70174, Stuttgart, Germany
h-j.massonne@imi.uni-stuttgart.de

ABSTRACT

A Late Jurassic seafloor remnant of the Rocas Verdes basin in southern Chile, the Sarmiento Complex (*ca.* 52°S), bears lithological layers with bimodal meta-igneous rocks appropriate for a comprehensive investigation of magma genesis in part of a lateral lithological transition from continental rifting to initial seafloor spreading. Metamorphosed mafic rocks collected from different layers in the ophiolite pseudostratigraphy and a plagiogranite have positive εNd_{150} values (+ 1 and +2). Granophyres, which are crosscut by ophiolitic mafic dikes, have negative εNd_{150} values (-5). Dacitic dikes within thick successions of pillow basalt have the least negative εNd_{150} values (-3 and -4). Although mafic and felsic igneous rocks show contrasting isotopic signatures, thermochemical modeling (EC-AFC) suggests they can share a common origin. Models consider an arbitrary composition of the crustal assimilant (mostly metapelite with an average εNd_{150} value of -7) and evaluate the feasibility for generation of silicic melts through the interaction of mafic magmas and metasedimentary rocks. A quantitative evaluation of basaltic magma contaminated by crustal wall rocks requires a Ma^*/Mc (mass of anatectic melt/ mass of cumulates) ratio of 0.04. Analyses using dikes of dacite (with Ma^*/Mc ratios ranging between 0.28-0.35) and granophyres (with Ma^*/Mc ratios of 0.63-0.89) require the silicic magmas to contain higher proportions of anatectic melts derived from metamorphic rocks. Isotopic differences among granophyres and dacites could be controlled by eruption dynamics, regional stress field and/or differences in thermal regimes in magma chambers. Bimodal magmatism in the earliest tectonic evolution of the Rocas Verdes basin could reflect regimes of slow extension of the continental crust along the Jurassic southwestern margin of Gondwana.

Key words: Rocas Verdes basin, Sarmiento Complex, Bimodal magmatism, Petrogenesis, Patagonia, Chile.

RESUMEN

Interacciones corteza-manto y generación de fundidos silíceos: perspectivas desde el Complejo Sarmiento, Andes patagónicos australes. Un remanente Jurásico del fondo oceánico de la cuenca de Rocas Verdes, el Complejo Sarmiento (*ca.* 52°S), contiene niveles con asociaciones de rocas bimodales apropiadas para la

investigación de la génesis de magmas en parte de la transición litológica entre 'rifting' continental y etapas tempranas de la extensión oceánica. Rocas máficas metamorfizadas y plagiogranitos en distintos niveles de la pseudoestratigrafía ofiolítica, tienen valores positivos de εNd_{150} (+1 and +2). Granófiros, que se encuentran atravesados por diques máficos con afinidades ofiolíticas, tienen valores negativos de εNd_{150} (-5). Diques de dacita que intruyen una sucesión de basaltos almohadillados también presentan valores de εNd_{150} negativos (-3 y -4). Aunque las rocas estudiadas muestran razones isotópicas contrastantes, un modelo termoquímico, energéticamente balanceado (EC-AFC) sugiere que ellas pueden compartir un origen en común. Los modelos consideran una composición arbitraria de asimilante cortical (principalmente metapelita con un valor promedio de εNd_{150} cercano a -7) y evalúa la posibilidad de generación de magmas silíceos a través de la interacción de magmas máficos y rocas metasedimentarias. Una evaluación cuantitativa de la contaminación de magma basáltico por rocas encajantes, indica razones de Ma*/Mc (masa de líquido anatéctico/ masa de cumulados) de 0,04. En cambio, análisis cuantitativos en diques de dacita (con Ma*/Mc entre 0,28-0,35) y granófiros (con Ma*/Mc entre 0,63-0,89), indican que magmas silíceos contienen mayor proporción de líquidos antécticos derivados de rocas metamórficas. Las diferencias isotópicas entre granófiros y dacitas podrían haber sido controladas por la dinámica de la erupción, régimen de esfuerzos tectónicos y/o por diferencias de regímenes termales en la cámara magmática. El magmatismo bimodal en las etapas tempranas de la evolución de la cuenca de Rocas Verdes, probablemente refleja regímenes con bajas tasas de extensión en la corteza continental del margen sudoccidental de Gondwana durante el Jurásico.

Palabras Claves: Cuenca Rocas Verdes, Complejo Sarmiento, Magmatismo bimodal, Petrogénesis, Patagonia, Chile.

INTRODUCTION

Crust-mantle interactions involve processes of mass, chemical and thermal exchange between mantle-derived basaltic magmas and crustal metamorphic rocks. Basaltic injection into the crust has been widely considered as an important mechanism to generate silicic melts in the continental and oceanic crust (*e.g.*, Huppert and Sparks, 1988; Pankhurst and Rapela, 1995; Petford and Gallagher, 2001). Basalt can act either as a parental source or as the thermal trigger for crustal melting (Grunder, 1995). The latter process is controlled by the fertility of the crustal material, temperature and the water content of basaltic magma (Annen and Sparks, 2002). Evidences from field and geochemical studies and experimental petrology point to amphibolite, metapelite and metagreywacke as suitable crustal lithologies for partial melting and generation of silicic melts (*e.g.,* Wolf and Wyllie, 1994; Rapp and Watson, 1995; Patiño Douce and Beard, 1995; Milord *et al.*, 2001). Even partial melting experiments performed with mixtures of dry basalt and metapelite yielded water-undersatured granitic melts (Patiño Douce, 1995) at temperatures of 1,000°C and 5-15 kbar pressure.

Several ophiolite complexes and overlying hemipelagic sedimentary successions exposed along the southern Pacific margin of South America (Fig. 1) have been considered as seafloor remnants of the Late Jurassic-Early Cretaceous Rocas Verdes basin (Katz, 1964; Dalziel *et al.*, 1974; Suárez and Pettigrew, 1976; Fuenzalida and Covacevich, 1988; Stern and de Wit, 2003). The Sarmiento Complex preserves a lithological pseudostratigraphy with mixed mafic-felsic layers and without the ultramafic components of 'classical' ophiolites. De Wit and Stern (1981) argued for its development over a diffuse zone, dominated by the interaction between mafic magmas and continental rocks, when two continental blocks were separated. SHRIMP U-Pb zircon geochronology constrain bimodal volcanism to the time from 152 to 147 Ma (Calderón, 2006; Calderón *et al.,* in press) enhancing the Sarmiento Complex as a geological setting where petrological and tectonic aspects of bimodal magmatism and continental lithosphere rupturing can be studied. For this purpose, whole rock Sr and Nd isotopic ratios, mineral chemistry and $^{40}Ar/^{39}Ar$ ages have been obtained in an appropriate suite of rocks collected over several field seasons. The use of Nd isotopic ratios and the thermodynamic framework of the energy-constrained assimilation fractional-crystallization (EC-AFC) model for complex open magmatic systems (Spera and Bohrson, 2001) provide petrological and thermochemical insights into the generation of silicic magmas through the interaction of basalt and fertile metamorphic rocks.

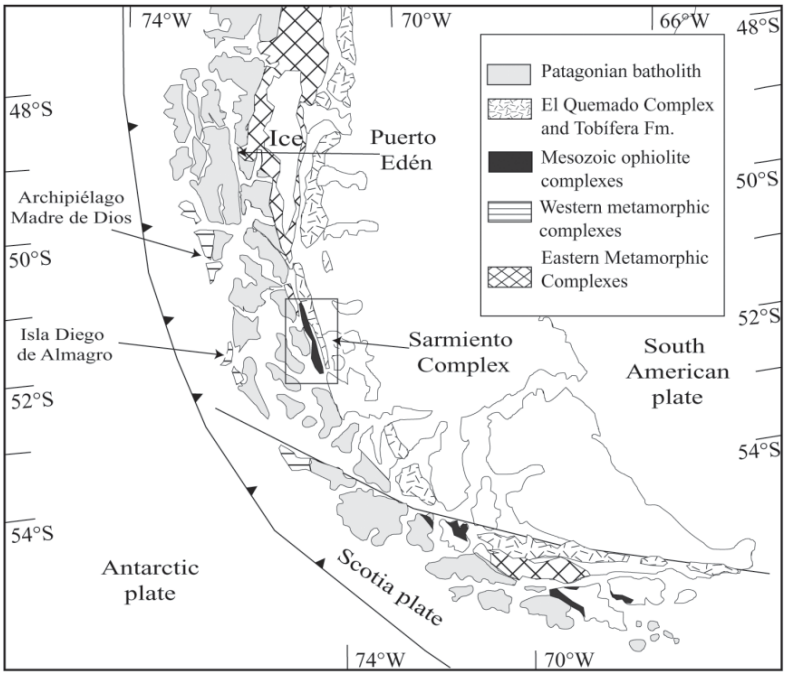

FIG. 1. Location map of the geological units in the southwestern Patagonian and Fuegian Andes.

GEOLOGICAL BACKGROUND

The Sarmiento Complex formed as part of a submarine and partitioned basin that was continuously filled with the hemipelagic sedimentary successions known as the 'black shales' of the Zapata Formation (Allen, 1982; Fildani and Hessler, 2005). Basin development involved widespread eruptions of subaerial and subaquatic felsic ignimbrites that were deposited in the fault-bounded grabens of the basin associated with the El Quemado Complex (*ca.* 155 Ma; Pankhurst *et al.*, 2000) and the Tobífera Formation (*ca.* 148-142 Ma; Calderón *et al.*, in press). The Rocas Verdes basin evolved to a backarc basin in Early Cretaceous times (Wilson, 1991; Calderón, 2006) when rhythmic successions of fine grained distal turbidites in the upper member of the Zapata Formation (cf. Fuenzalida and Covacevich, 1988) were deposited. Basin closure and obduction onto the cratonic margin occurred in the mid-Cretaceous (Dalziel, 1981) before the main orogenic deformation and rapid uplift of the Andean mountain chain leading to the initiation of the Magallanes foreland basin at ~92 Ma (Fildani *et al.*, 2003).

The formation of the Sarmiento Complex was contemporaneous in part with the emplacement of the Late Jurassic and eastern plutonic belt of the South Patagonian batholith (Fig.1), which is mainly composed of leucogranite with some gabbro (Hervé *et al.*, 2007). Narrow and discontinuous belts of andalusite and sillimanite gneisses as well as migmatites occur in close spatial relation to the granitic belt (Watters, 1964; Calderón, 2005). A Late Jurassic age for crustal anatexis has been established through dating of overgrowth zones of zircons from the sillimanite gneisses (Hervé *et al.,* 2003). At the Puerto Edén Igneous and Metamorphic Complex (Fig. 1), granites are considered as mixtures of variable amounts of radiogenic crust-derived anatectic melts and less radiogenic mafic magmas (Calderón *et al.*, 2007).

Late Paleozoic polydeformed metasedimentary rocks, grouped in the Staines Complex and the Eastern Andean Metamorphic Complex (Forsythe

and Allen, 1980; Hervé *et al*., 1998; Hervé *et al*., 2003; Augustsson, 2003; Augustsson *et al*., 2006), crop out to the east of the South Patagonian batholith (Stewart *et al*., 1971)[1]. To the west of the batholith (at Archipiélago Madre de Dios; Fig. 1) thick successions of limestone, basalt and chert are thought to represent fragments of seamounts accreted to the paleo-Pacific margin of Gondwana (Forsythe and Mpodozis, 1983) between Early Permian and Early Jurassic times (Thomson and Hervé, 2002). The turbidites of the Duque de York Complex were deposited on top of the limestone- and basalt- successions between post-Early Permian to pre-Early Jurassic times in an active margin setting (Faúndez *et al.,* 2002; Lacassie *et al*., 2006). The Diego de Almagro Metamorphic Complex, that crops out to the west and is separated from the Duque de York complex by the northwest-southeast trending Seno Arcabuz shear zone (Olivares *et al*., 2003), consists of foliated meta-granite, paraschists and blueschists juxtaposed in a subduction zone setting in the Early Cretaceous (Willner *et al*., 2004).

OCURRENCE AND MINERALOGY OF STUDIED SAMPLES

Samples for this study were collected from the pre-Jurassic metasedimentary rocks of the Staines Complex, the bimodal meta-igneous rocks of the Sarmiento Complex, felsic metamorphosed tuffs of the Tobífera Formation and late small volume igneous rocks in the Sarmiento Complex.

STAINES COMPLEX

Greenschist facies psammopelitic schists of the Staines Complex (Stewart *et al*., 1971[1]; Forsythe and Allen, 1980; Allen, 1982; Hervé *et al*., 2003) crop out to the west of the Sarmiento Complex (Fig. 2). They consist of fine-grained and polydeformed white-mica chlorite schists with folded and crenulated millimeter- to centimeter-wide bands of granoblastic quartz and restricted plagioclase. Minor amounts of chloritized blasts of biotite also occur. Tourmaline, zircon, apatite and opaque such as graphite and Fe-Ti oxides are accessory phases. The turbiditic protolith of meta-morphic rocks was deposited in the late Paleozoic (Hervé *et al*., 2003; Augustsson *et al.,* 2006).

SARMIENTO COMPLEX

In the southern segment of the Sarmiento Complex the incomplete ophiolite pseudostratigraphy dips gently to the south. Metagabbros (sills and dikes) and plagiogranites occur in the northern parts of the complex (Seno Lolos), whereas extrusive rocks dominate the southern exposures to Canal Unión (Fig. 2). Field work in the Sarmiento Complex has shown that it is possible to distinguish three main lithological layers in the region, as discussed below:

1. A mafic extrusive layer: exposed along the Cordillera Sarmiento is composed of a kilometer-thick, flat-lying succession of pillow and massive basalt, pillow breccias, and restricted intercalations of radiolaria-bearing cherts and siltstones. Olivine basalts show porphyritic and branching textures with metamorphic assemblages consisting of pumpellyite, chlorite, quartz, plagioclase, epidote, titanite, carbonate and rare actinolite. Metamorphic phases occur in amygdules, phenocrysts, veins and the groundmass. Olivine is totally replaced by calcite and/or chlorite. Clinopyroxene is the only relict mafic igneous phase. Meter-wide dikes of fine grained dolerite composed mainly of subhedral plagioclase (35-45%), ophitic clinopyroxene (25-35%), inter-stitial chlorite (13-23%) and accessory quartz, titanite and epidote occur in this layer.

2. A mafic-felsic extrusive layer: exposed along Península Taraba and at Isla Young consists mainly of successions of pillow basalts with intercalations of silicic tuffs and hyaloclastites. These successions are cut by late meter-wide dikes of dacite and rhyolite. Porphyritic and amygdaloidal basalts show variable amounts (5-15%) of olivine phenocrysts that are totally retrogressed to chlorite. In some cases, they contain calcite. A branching texture in the groundmass is defined by an aggregate of plagioclase, clinopyroxene, interstitial chlorite, accessory Fe-Ti oxides and pyrite. Felsic dikes are porphyritic rocks with phenocrysts of embayed quartz and subhedral plagioclase, and accessory allanite and chloritized pseudomorphs. Some of these rocks are partially brecciated and have myarolitic cavities suggesting hypabyssal conditions during crystalliza-

[1] Stewart, J.; Cruzat, A.; Page, B.; Suárez, M.; Stambuk, V. 1971. Estudio geológico económico de la Cordillera Patagónica entre los paralelos 51°00" y 53°30" Lat.S, provincia de Magallanes. Instituto de Investigaciones Geológicas (Inédito): 174. Santiago, Chile.

tion. The quarzofeldspathic and spherulitic groundmass is aphanitic. Apatite and zircon are accessory phases. The secondary assemblage consists of chlorite, epidote, quartz and feldspars.

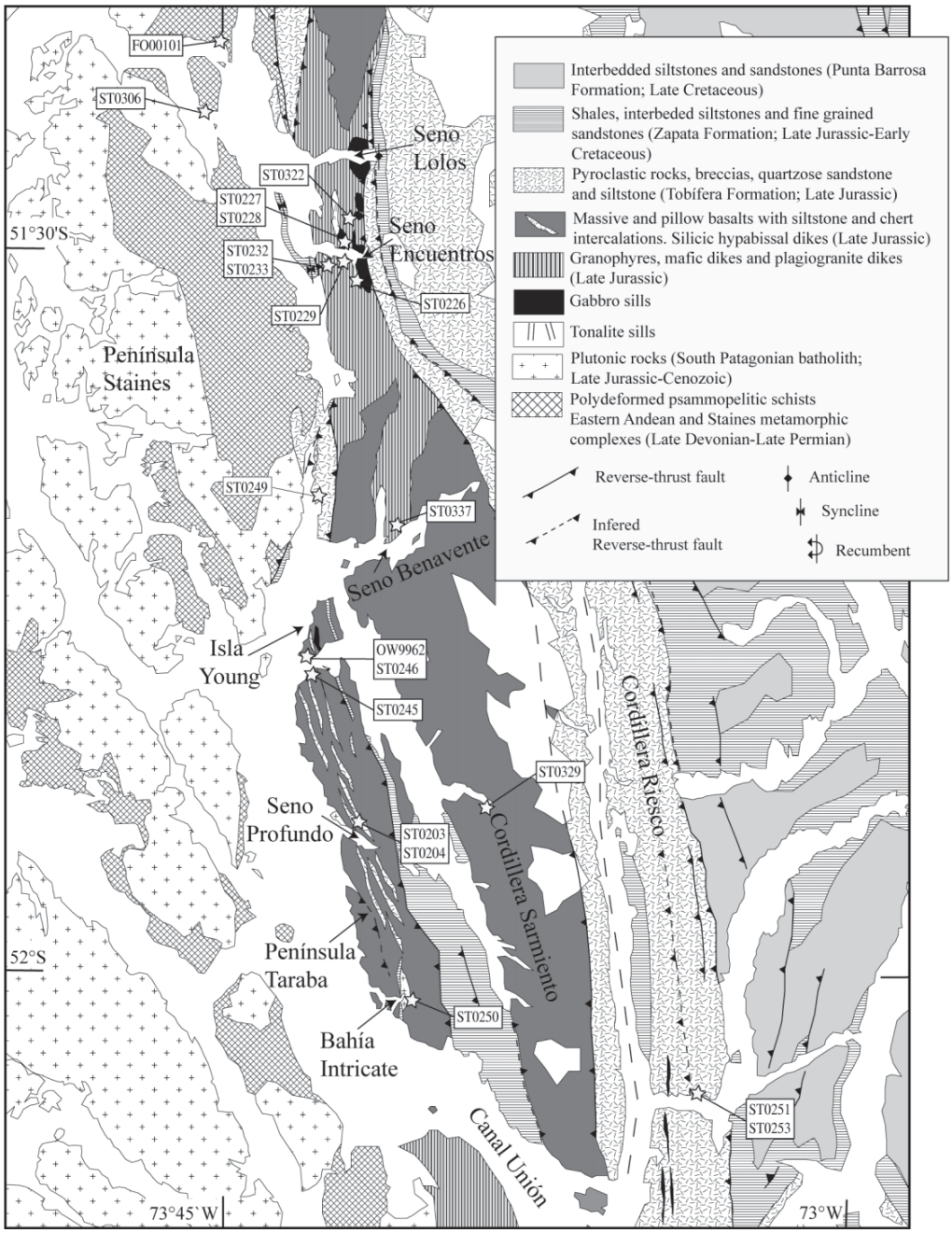

FIG. 2. Geological map of the Cordillera Sarmiento and surrounding areas (modified from Allen 1982 and Stewart *et al.*, 1971[1]). Main localities and the location of samples are shown. If more than one sample was collected in a single locality, numbers are followed by capital letters.

The mafic-felsic extrusive layer includes a narrow belt of sheared felsic and mafic meta-igneous rocks with a north-northwest trending subvertical foliation. The metamorphic assemblage in strain fringes and other microstructures in mafic rocks consists of actinolite, quartz, plagioclase, chlorite and titanite. In the foliated felsic rocks, the predominant metamorphic phases are chlorite, epidote, titanite, quartz and feldspar with minor amounts of white mica. At the southern tip of Península Taraba (Bahía Intricate; Fig. 2), a small pluton of fine-grained biotite tonalite is in contact with massive, hornfelsic basalts and the folded sedimentary successions of the Zapata Formation. The biotite tonalite contains microscopic inclusions of metamorphic rocks composed of quartz, plagioclase and decussate biotite.

3. A mafic-felsic intrusive layer: exposed between the east-west trending Seno Lolos, Seno Encuentros and along the northern shore of Seno Benavente (Fig. 2), consists of fine to medium-grained plagioclase- and quartz-rich porphyritic rocks with granophyric and graphic textures, hereinafter called granophyres. They are characterized by the presence of accessory allanite with narrow and irregular rims of colorless epidote. The granophyres are intruded by a swarm of north-south trending subvertical dike complexes of coarse- and fine-grained metagabbro. The dikes have intergranular textures with no preserved pyroxene. Although most mafic dikes are straight and show centimeter-wide chilled margins, some sinusoidal dikes occur. Sheeted dike complexes occur in higher topographic levels (deWit and Stern, 1981). Rare fine-grained plagiogranite dikes are in subhorizontal contact with subvertical mafic dikes. The plagiogranite dikes are composed of plagioclase, quartz and metamorphic epidote and chlorite. At the base of the mafic-felsic intrusive layer, homogeneous medium-grained and 'amphibolitized' gabbroic sills or dikes are found that preserve intergranular and cumulate textures that are defined by interlocking tabular plagioclase and xenomorphic hornblende. Interstitial opaque minerals are Fe-Ti oxides and pyrite. Sills of hornblende tonalite with inclusions of amphibolite and mafic aphanitic rocks appear at the base of this layer. The amphibolites have granoblastic textures with amphibole and plagioclase (melanosome) and leucocratic veins of tonalite (leucosome). Hornblende grains in the melanosomes have scarce relict inclusions of clinopyroxene. Hornblende in the amphibolites is retrogressed to actinolite, chlorite, titanite, epidote and traces of biotite. Plagioclase, in some cases, is replaced by microcrystals of white mica.

LATE SMALL VOLUME HORNBLENDE-BEARING INTERMEDIATE ROCKS

Plutons of medium-grained and panhypidiomorphic hornblende tonalite with marginal granodiorite components crop out at Seno Encuentro (Fig. 2). Porphyritic and medium-grained hornblende dacitic dikes, with subhedral phenocrysts of hornblende, plagioclase and quartz within an afanitic quartzofeldspathic groundmass occur at Seno Benavente. The hornblende in them is partially replaced by chlorite, epidote and carbonate. Plagioclase shows variable degree of sericitization.

TOBÍFERA FORMATION

Along the eastern flank of the Cordillera Sarmiento and the main part of the Cordillera Riesco, a kilometer-wide, north-south trending belt of sheared silicic pyroclastic rocks intercalated with meter-sized horizons of sheared quartz-bearing siltstones has been mapped in the Tobífera Formation (Stewart *et al.*, 1971[1]; Bruhn *et al.*, 1978; Allen, 1982; Galaz *et al.,* 2005). These meta-rhyolites have crystallization ages of *ca.* 148 Ma (SHRIMP U-Pb zircon ages; Calderón, 2006). Geothermobarometry of syntectonic metamorphic assemblages consisting of phengite, chlorite, stilpnomelane, and quartz indicate medium pressure greenschist facies conditions during dynamic metamorphism (Hervé *et al.*, 2004; Calderón *et al.*, 2005). The sheared belt is intruded by meter-wide, north-south trending sills of medium-grained chloritized dolerite, that (in studied samples) show no evidence of dynamic recrystallization. Consequently, the injection of the mafic magmas in this belt occurred after shearing and, is not related to the *ca.* 150 Ma old mafic magmatic events.

Tobífera rocks crop out to the west and in thrust contact over the Sarmiento Complex. They share an unconformable depositional contact with Paleozoic metasedimentary rocks that are basal breccias and conglomerates intercalated with greywackes, sandstones, siltstones. Rhyolitic crystal lapilli tuffs are dominant in the upper part of the succession (Allen, 1982). Minor lithic fragments of metasedimentary rocks and porphyritic rocks that are common constituents in these pyroclastic

rocks show discrete stylolitic bands and anastomosing cleavages indicating dynamic recrystallization that is less intense than in the eastern sheared belt. White mica, quartz and plagioclase constitute the metamorphic assemblage. Pyrite is a frequent opaque phase.

MINERAL PHASE CHEMISTRY OF METAMORPHOSED MAFIC ROCKS

Mineral compositions were measured at the Institut für Mineralogie und Kristallchemie, Universität Stuttgart, using a CAMECA SX-100 microprobe with 5 wavelength-dispersive systems. Operating conditions were: 15kV and 15 nA, a beam size of 7-10 μm or a focussed beam (for very small crystals), 20 seconds counting time on the peak and on the background for each element. The standards used were natural wollastonite (Si, Ca), natural orthoclase (K), natural albite (Na), natural rhodonite (Mn), synthetic Cr_2O_3 (Cr), synthetic TiO_2 (Ti), natural hematite (Fe), natural baryte (Ba), synthetic MgO (Mg), synthetic Al_2O_3 (Al) and synthetic NiO (Ni). The PaP correction procedure provided by Cameca was applied.

The analyses were chosen to illustrate the compositional ranges of pyroxene, plagioclase and amphibole found in the metamorphosed mafic rocks. Studied samples were two medium-grained amphibolitized metagabbros (samples ST0228 and ST0229A) collected from the mafic-felsic intrusive layer. An amphibolite, consisting of an amphibole-rich melanosome and a quartz-plagioclase leucosome was also analyzed (sample ST0226A). A fine-grained and weakly foliated dike of metabasaltic-andesite (ST0204) and an olivine metabasalt (OW9962) with lath-shaped crystals of plagioclase and needles of clinopyroxene in the groundmass were collected from the mafic-felsic extrusive layer. Mineral compositions are presented in tables 1-3. The location of studied samples is illustrated in figure 2.

PYROXENE

Partially affected by metamorphic processes, clinopyroxene, which is predominantly augite in composition (Fig. 3), shows variable Mg-number [(100*Mg/ (Mg+Fe^{2+})] and minor element concentrations. No compositional variation was detected where relict crystals allowed core and rim domains to be analyzed (see analyses of samples ST0204 and ST0228 in table 1). Clinopyroxene is the main

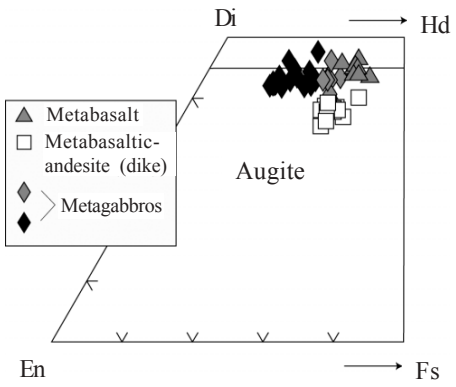

FIG. 3. Pyroxene quadrilateral plots for the ophiolitic metamorphosed mafic rocks of the Sarmiento Complex.

stable igneous phase in the mafic rocks and its chemistry reflects primary magmatic compositions.

The most primitive pyroxene grains, found in metagabbro ST0228, have Mg-numbers ranging from 80 to 90 in most cases and Cr_2O_3 contents as high as 0.36 wt% (Fig. 4a). Lower Mg-numbers in pyroxenes in the other metagabbro ST0229A suggest crystallization from a more fractionated magma. The clinopyroxene in both the dikes and lavas have Mg-number that range from approximately 67 to 75. Metabasalt OW9962 has clinopyroxene with conspicuously higher contents of TiO_2 and Al_2O_3, and elevated Na_2O contents relative to other lithologies (Figs. 4b-d). These clinopyroxene crystals also have higher Cr_2O_3 contents than those in the metabasaltic-andesite and the evolved metagabbro. Although a negligible acmite component is found in the clinopyroxene, sodium contents show a good correlation with Mg-number (Fig. 4d).

PLAGIOCLASE

All of the plagioclase in the metabasalts and metabasaltic-andesites is albite in composition (Fig. 5) indicating a metamorphic origin. The albite

TABLE 1. REPRESENTATIVE CHEMICAL ANALYSES OF PYROXENE IN METAMORPHOSED MAFIC ROCKS (O=6).

Sample	OW9962 (metabasalt)				ST0204 (metabasaltic-andesite)							ST0228 (metagabbro)							ST0229A (metagabbro)			
Spot	3	4	5	6	72	25	66	61	63	60	64	28	32	76	74	31	33	85	28	19	27	2
							rim	rim	rim	core	core		core	core	rim	rim	rim					
SiO_2	46.31	46.13	45.98	45.58	49.45	49.66	49.78	49.97	50.28	50.34	50.77	52.27	52.16	51.68	51.43	51.41	50.25	49.85	51.52	51.36	50.59	50.07
TiO_2	2.55	2.70	2.76	2.87	0.74	0.84	0.83	0.83	0.87	0.72	0.80	0.32	0.45	0.44	0.62	0.52	0.95	0.93	0.28	0.25	0.54	0.65
Al_2O_3	6.23	5.20	5.69	6.89	1.68	1.95	2.51	1.92	2.29	2.42	2.06	1.06	2.37	2.53	1.94	1.81	2.55	2.39	1.13	0.81	1.68	1.90
Cr_2O_3	0.13	0.21	0.21	0.19	0.00	0.00	0.01	0.00	0.00	0.02	0.02	0.17	0.19	0.36	0.13	0.29	0.14	0.02	0.02	0.02	0.03	0.03
FeO	11.76	13.57	12.02	11.72	14.13	12.70	11.79	12.84	11.94	11.99	11.79	6.52	6.49	6.27	8.07	6.49	8.98	8.72	10.73	11.74	10.69	10.13
MnO	0.26	0.36	0.26	0.24	0.35	0.35	0.33	0.32	0.32	0.27	0.31	0.25	0.15	0.16	0.19	0.18	0.27	0.27	0.28	0.31	0.30	0.33
MgO	11.06	11.13	11.46	11.49	12.63	14.03	14.22	14.44	14.64	14.22	14.32	15.50	16.73	16.84	15.46	16.34	15.10	14.51	13.80	13.13	13.77	13.86
CaO	21.47	20.31	20.69	20.65	19.40	18.68	18.85	18.49	18.42	18.44	19.02	23.01	20.86	21.15	21.58	21.58	20.43	21.74	21.28	21.30	20.95	20.75
Na_2O	0.33	0.37	0.33	0.36	0.25	0.23	0.35	0.23	0.27	0.31	0.28	0.19	0.21	0.23	0.26	0.16	0.26	0.32	0.32	0.31	0.32	0.35
K_2O	0.00	0.01	0.01	0.02	0.01	0.00	0.01	0.01	0.00	0.02	0.02	0.03	0.00	0.00	0.00	0.00	0.01	0.01	0.01	0.00	0.01	0.05
NiO	0.05	0.01	0.04	0.00	0.00	0.00	0.01	0.00	0.00	0.00	0.00	0.00	0.00	0.00	0.00	0.00	0.00	0.00	0.00	0.00	0.00	0.00
Total	100.15	99.99	99.45	99.99	98.64	98.44	98.69	99.06	99.04	98.76	99.38	99.32	99.62	99.66	99.68	98.77	98.95	98.76	99.37	99.22	98.87	98.12
Si	1.749	1.754	1.749	1.720	1.898	1.894	1.886	1.892	1.898	1.907	1.912	1.941	1.919	1.899	1.907	1.912	1.883	1.873	1.939	1.946	1.913	1.904
Aliv	0.251	0.233	0.251	0.280	0.076	0.088	0.112	0.086	0.102	0.093	0.088	0.046	0.081	0.101	0.085	0.079	0.113	0.106	0.050	0.036	0.075	0.085
Ti	0.073	0.077	0.079	0.081	0.021	0.024	0.024	0.024	0.025	0.021	0.023	0.009	0.013	0.012	0.017	0.015	0.027	0.026	0.008	0.007	0.015	0.018
Alvi	0.026	0.000	0.004	0.027	0.000	0.000	0.000	0.000	0.000	0.015	0.003	0.000	0.022	0.008	0.000	0.000	0.000	0.000	0.000	0.000	0.000	0.000
Fe^{3+}	0.100	0.125	0.107	0.111	0.105	0.094	0.095	0.101	0.073	0.060	0.060	0.064	0.042	0.075	0.082	0.070	0.083	0.119	0.080	0.080	0.091	0.098
Cr	0.004	0.006	0.006	0.006	0.000	0.000	0.000	0.000	0.000	0.001	0.000	0.005	0.006	0.010	0.004	0.009	0.004	0.001	0.001	0.000	0.001	0.001
Fe^{2+}	0.275	0.311	0.279	0.262	0.353	0.314	0.282	0.309	0.306	0.322	0.313	0.139	0.158	0.119	0.170	0.133	0.200	0.158	0.260	0.294	0.249	0.227
Mn	0.008	0.012	0.008	0.008	0.011	0.011	0.011	0.010	0.010	0.009	0.010	0.008	0.005	0.005	0.006	0.006	0.009	0.009	0.009	0.010	0.010	0.010
Mg	0.623	0.631	0.650	0.647	0.723	0.798	0.803	0.815	0.824	0.803	0.804	0.858	0.918	0.923	0.854	0.906	0.844	0.813	0.774	0.742	0.776	0.786
Ca	0.869	0.827	0.843	0.835	0.798	0.763	0.765	0.750	0.745	0.749	0.767	0.915	0.822	0.832	0.858	0.860	0.820	0.875	0.858	0.864	0.849	0.845
Na	0.024	0.027	0.024	0.026	0.019	0.017	0.025	0.017	0.020	0.023	0.020	0.014	0.015	0.017	0.019	0.012	0.019	0.024	0.024	0.023	0.024	0.026
K	0.000	0.000	0.000	0.001	0.000	0.000	0.000	0.000	0.000	0.001	0.001	0.001	0.000	0.000	0.000	0.000	0.001	0.000	0.000	0.000	0.000	0.003
Ni	0.001	0.000	0.001	0.000	0.000	0.000	0.000	0.000	0.000	0.000	0.000	0.000	0.000	0.000	0.000	0.000	0.000	0.000	0.000	0.000	0.000	0.000
Total	4.003	4.005	4.003	4.003	4.004	4.003	4.003	4.003	4.002	4.002	4.002	4.001	4.001	4.001	4.002	4.001	4.002	4.003	4.002	4.002	4.003	4.003
Mg-No.	69	67	70	71	67	72	74	73	73	71	72	86	85	89	83	87	81	84	75	72	76	78

[mg]=100*Mg/(Mg+Fe^{2+})

TABLE 2. REPRESENTATIVE CHEMICAL ANALYSES OF PLAGIOCLASE IN METAMORPHOSED MAFIC ROCKS (O=8).

Sample	OW9962 (metabasalt)			ST0204 (metabasaltic-andesite)				ST0228 (metagabbro)					ST0229A (metagabbro)				
Spot	**1**	**2**	**3**	**71**	**10**	**14**	**5**	**79**	**18**	**40**	**23**	**65**	**12**	**46**	**16**	**3**	**48**
SiO_2	68.43	68.87	68.63	68.59	68.85	69.07	69.29	52.43	46.75	46.59	46.07	45.69	64.17	55.80	51.94	51.62	50.40
TiO_2	0.00	0.00	0.01	0.01	0.03	0.01	0.01	0.06	0.03	0.03	0.02	0.03	0.03	0.03	0.06	0.07	0.05
Al_2O_3	20.56	20.00	19.95	21.13	20.94	21.23	21.30	29.24	32.55	32.58	33.23	33.67	23.66	27.46	29.29	29.83	30.52
Cr_2O_3	0.00	0.04	0.03	0.00	0.00	0.00	0.01	0.00	0.01	0.00	0.01	0.00	0.00	0.00	0.00	0.00	0.01
FeO	0.18	0.16	0.12	0.15	0.20	0.33	0.37	0.46	0.71	0.67	0.62	0.63	0.25	0.44	0.56	0.56	0.53
MnO	0.04	0.02	0.04	0.00	0.01	0.01	0.00	0.00	0.02	0.00	0.01	0.00	0.03	0.00	0.00	0.00	0.01
MgO	0.04	0.03	0.02	0.00	0.00	0.00	0.00	0.05	0.04	0.04	0.02	0.02	0.01	0.06	0.05	0.09	0.03
CaO	0.41	0.49	0.12	0.43	0.39	0.44	0.71	12.27	16.33	16.62	17.09	17.69	3.87	9.77	12.81	12.89	13.88
Na_2O	11.42	11.58	12.14	11.04	11.27	11.42	10.09	4.86	2.39	2.28	2.04	1.65	9.06	6.25	4.50	4.59	4.04
K_2O	0.39	0.16	0.09	0.10	0.05	0.08	0.06	0.19	0.05	0.09	0.06	0.05	0.13	0.12	0.08	0.16	0.09
Total	101.49	101.36	101.14	101.46	101.73	102.59	101.85	99.56	98.89	98.91	99.17	99.43	101.20	99.92	99.27	99.81	99.57
Si	2.955	2.975	2.973	2.952	2.956	2.946	2.962	2.396	2.179	2.173	2.145	2.124	2.798	2.519	2.382	2.359	2.315
Ti	0.000	0.000	0.000	0.000	0.001	0.000	0.000	0.002	0.001	0.001	0.001	0.001	0.001	0.001	0.002	0.002	0.002
Al	1.047	1.018	1.018	1.072	1.060	1.067	1.073	1.575	1.788	1.791	1.824	1.845	1.216	1.461	1.583	1.607	1.652
Cr	0.000	0.001	0.001	0.000	0.000	0.000	0.000	0.000	0.000	0.000	0.000	0.000	0.000	0.000	0.000	0.000	0.000
Fe	0.007	0.006	0.004	0.005	0.007	0.012	0.013	0.018	0.028	0.026	0.024	0.024	0.009	0.017	0.021	0.021	0.021
Mn	0.002	0.001	0.001	0.000	0.000	0.000	0.000	0.000	0.001	0.000	0.000	0.000	0.001	0.000	0.000	0.000	0.001
Mg	0.002	0.002	0.001	0.000	0.000	0.000	0.000	0.004	0.003	0.002	0.002	0.002	0.000	0.004	0.003	0.006	0.002
Ca	0.019	0.023	0.006	0.020	0.018	0.020	0.033	0.601	0.815	0.831	0.853	0.881	0.181	0.472	0.629	0.631	0.683
Na	0.956	0.970	1.020	0.921	0.938	0.944	0.836	0.430	0.216	0.206	0.184	0.149	0.766	0.547	0.400	0.407	0.360
K	0.022	0.009	0.005	0.005	0.002	0.004	0.003	0.011	0.003	0.005	0.004	0.003	0.007	0.007	0.005	0.010	0.005
Total	5.010	5.005	5.030	4.975	4.983	4.994	4.921	5.036	5.035	5.036	5.036	5.028	4.979	5.027	5.026	5.043	5.040
An	1.92	2.26	0.55	2.10	1.85	2.08	3.74	57.64	78.79	79.68	81.95	85.33	18.96	46.04	60.88	60.26	65.16
Ab	95.91	96.88	98.98	97.34	97.89	97.49	95.86	41.31	20.90	19.80	17.68	14.41	80.28	53.30	38.67	38.83	34.36
Or	2.17	0.86	0.47	0.57	0.26	0.43	0.40	1.06	0.31	0.51	0.37	0.26	0.76	0.65	0.45	0.91	0.48

TABLE 3. REPRESENTATIVE CHEMICAL ANALYSES OF AMPHIBOLE IN METAMORPHOSED MAFIC ROCKS (O=23).

Sample	ST0204 (metabasaltic-andesite)					ST0228 (metagabbro)											
Spot Nª	13	28	30	37	39	15	2	6	83	61	51	56	11	41	84	23	1
SiO_2	48.43	49.92	50.28	53.12	53.84	55.36	54.92	53.87	53.87	53.82	53.65	53.02	52.72	51.46	50.90	54.04	53.
TiO_2	0.04	0.02	0.03	0.01	0.02	0.20	0.09	0.16	0.23	0.12	0.12	0.16	0.18	0.23	0.74	0.11	0.
Al_2O_3	4.03	2.51	2.40	1.05	0.98	1.29	1.15	1.36	1.14	2.56	2.17	2.52	2.67	3.77	3.60	1.33	1.
Cr_2O_3	0.00	0.01	0.00	0.01	0.00	0.08	0.10	0.03	0.05	0.02	0.01	0.01	0.02	0.14	0.32	0.01	0.
FeO	19.19	17.64	18.18	16.38	16.22	6.59	8.44	10.23	11.44	9.86	10.15	11.10	11.83	11.08	10.50	15.11	12.
MnO	0.29	0.28	0.29	0.27	0.28	0.10	0.16	0.14	0.17	0.22	0.27	0.34	0.26	0.28	0.17	0.69	0.
MgO	10.86	12.96	12.54	13.35	13.19	20.29	20.25	17.60	16.80	17.83	17.92	17.36	16.97	16.63	16.47	17.13	16.
CaO	11.06	11.10	11.49	12.17	11.95	12.74	10.87	12.63	12.32	12.39	12.33	11.61	11.11	11.94	12.57	8.17	12.
Na_2O	0.71	0.49	0.58	0.42	0.39	0.14	0.13	0.14	0.16	0.33	0.31	0.46	0.35	0.64	0.20	0.33	0.
K_2O	0.72	0.14	0.23	0.08	0.10	0.04	0.16	0.05	0.03	0.05	0.02	0.04	0.06	0.06	0.05	0.02	0.
NiO	0.02	0.00	0.02	0.00	0.00	0.00	0.00	0.01	0.04	0.00	0.00	0.06	0.02	0.00	0.00	0.00	0.
H_2O	4.65	4.93	3.96	3.14	3.03	3.17	3.72	3.80	3.76	2.80	3.05	3.33	3.81	3.78	4.49	3.06	3.
Si	7.396	7.554	7.573	7.845	7.923	7.788	7.810	7.767	7.809	7.649	7.652	7.611	7.627	7.434	7.410	7.824	7.7
AlIV	0.604	0.446	0.426	0.155	0.077	0.212	0.190	0.231	0.191	0.351	0.348	0.389	0.373	0.566	0.590	0.176	0.2
sumT	8.000	8.000	7.999	8.000	8.000	8.000	8.000	7.998	8.000	8.000	8.000	8.000	8.000	8.000	8.000	8.000	7.9
AlVI	0.121	0.002	0.000	0.027	0.093	0.003	0.003	0.000	0.005	0.076	0.017	0.037	0.083	0.076	0.028	0.052	0.0
Ti	0.005	0.002	0.003	0.001	0.002	0.021	0.010	0.017	0.025	0.012	0.013	0.017	0.019	0.024	0.081	0.012	0.0
Fe^{3+}	0.326	0.274	0.204	0.088	0.044	0.123	0.100	0.142	0.096	0.240	0.277	0.309	0.237	0.398	0.342	0.115	0.1
Cr	0.000	0.001	0.000	0.001	0.000	0.009	0.011	0.004	0.006	0.002	0.001	0.001	0.002	0.016	0.036	0.001	0.0
Mg	2.473	2.924	2.816	2.939	2.894	4.255	4.293	3.783	3.631	3.778	3.811	3.715	3.659	3.582	3.575	3.698	3.5
Ni	0.002	0.000	0.002	0.000	0.000	0.000	0.000	0.001	0.004	0.000	0.000	0.006	0.002	0.000	0.000	0.000	0.0
Fe^{2+}	2.073	1.797	1.974	1.934	1.952	0.589	0.584	1.054	1.232	0.891	0.881	0.914	0.997	0.903	0.936	1.122	1.3
Mn	0.000	0.000	0.000	0.009	0.016	0.000	0.000	0.000	0.000	0.000	0.000	0.000	0.000	0.000	0.003	0.000	0.0
sumC	5.000	5.000	5.000	5.000	5.000	5.000	5.000	5.000	5.000	5.000	5.000	5.000	5.000	5.000	5.000	5.000	5.0
Mg	0.000	0.000	0.000	0.000	0.000	0.000	0.000	0.000	0.000	0.000	0.000	0.000	0.000	0.000	0.000	0.000	0.0
Fe^{2+}	0.052	0.161	0.111	0.000	0.000	0.064	0.321	0.038	0.058	0.041	0.052	0.109	0.197	0.038	0.000	0.592	0.0
Mn	0.038	0.036	0.037	0.025	0.019	0.011	0.019	0.017	0.021	0.027	0.032	0.041	0.032	0.034	0.018	0.085	0.0
Ca	1.810	1.800	1.852	1.925	1.884	1.920	1.655	1.945	1.913	1.887	1.885	1.786	1.722	1.847	1.960	1.267	1.9
Na	0.101	0.003	0.000	0.049	0.097	0.005	0.005	0.000	0.009	0.046	0.031	0.064	0.049	0.081	0.021	0.056	0.0
sum B	2.000	2.000	2.000	2.000	2.000	2.000	2.000	2.000	2.000	2.000	2.000	2.000	2.000	2.000	2.000	2.000	2.0
Ca	0.000	0.000	0.002	0.000	0.000	0.000	0.000	0.006	0.000	0.000	0.000	0.000	0.000	0.000	0.000	0.000	0.0
Na	0.109	0.140	0.169	0.071	0.014	0.032	0.032	0.039	0.037	0.046	0.054	0.065	0.050	0.096	0.036	0.038	0.0
K	0.140	0.027	0.044	0.015	0.019	0.008	0.030	0.008	0.005	0.009	0.004	0.007	0.012	0.012	0.008	0.003	0.0
sumA	0.249	0.167	0.216	0.086	0.033	0.040	0.062	0.053	0.042	0.054	0.058	0.072	0.061	0.108	0.044	0.041	0.0
total	15.249	15.167	15.215	15.086	15.033	15.040	15.062	15.051	15.042	15.054	15.058	15.072	15.061	15.108	15.044	15.041	15.0
$Mg/((Mg+Fe^{2+})$	0.54	0.60	0.57	0.60	0.60	0.87	0.83	0.78	0.74	0.80	0.80	0.78	0.75	0.79	0.79	0.68	0.
Ca/K	12.901	66.59	41.957	127.77	100.36	248.8	55.647	230.56	369.48	221.48	450.39	243.77	145.81	156.62	234.6	381.21	44

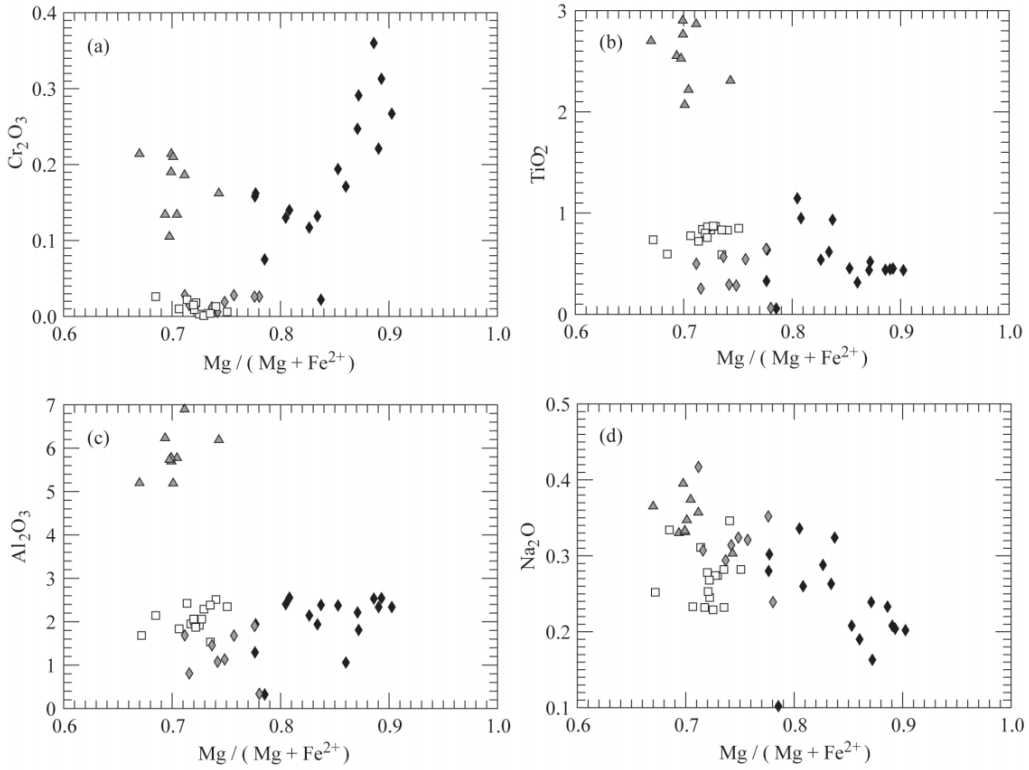

FIG. 4. Pyroxene Mg-number *versus* (a) Cr_2O_3, (b) TiO_2, (c) Al_2O_3, and (d) Na_2O.

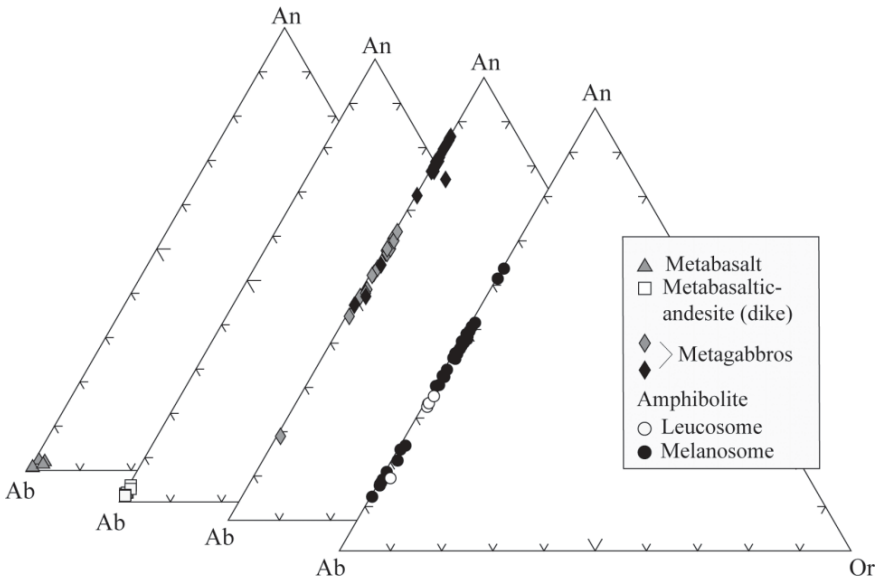

FIG. 5. Plagioclase Ab-Or-An ternary plots for plagioclases in metamorphosed mafic rocks.

occurs along with chlorite, epidote, titanite and scarce K-feldspar. The plagioclase in the metagabbros is predominantly bytownite (An_{73-87}; ST0228) and labradorite (An_{50-65}; ST0229A). Its composition and fresh aspect indicate that this feldspar is a primary igneous phase. The bytownite composition is consistent with the primitive character of sample ST0228, which is indicated by the high Mg-number and Cr_2O_3 content of the clinopyroxene.

Most plagioclase in the melanosome of the amphibolite is andesine (An_{37-51}). Some is oligoclase (An_{12-24}). The few crystals in the leucosomes that were analyzed are mostly andesine in composition (An_{32-35}).

AMPHIBOLE

Metamorphic amphibole in the studied samples is actinolite and magnesiohornblende (according to Leake *et al.*, 1997; Table 3). Actinolite in the mafic-extrusive layer is only present in the sheared domain, where sample ST0204 was collected. Actinolite is an ubiquitous phase in the mafic-felsic intrusive layer. Mg/(Mg+Fe) ratios are significantly higher in the actinolite in the metagabbros than in the metabasaltic-andesite (Fig. 6a). This feature is consistent with the progressive variation in Mg-number of relict clinopyroxene, indicating a bulk compositional control in the chemistry of actinolite. Some crystals of magnesiohornblende, which are usually replaced by aggregates of actinolite along crystal edges, occur in metagabbros.

The amphiboles in the amphibolite, both in the melanosome or leucosome, are magnesiohornblende. Those in the melanosome show lower silica contents (Si *ca.* 6.8 and 7.0 in tetrahedral site based on 23 oxygens; Fig 6a) than in the leucosome (tetrahedral Si 7.1 and 7.8). The composition of amphibole and plagioclase in granoblastic assemblages permits the use of the hornblende-plagioclase geothermometer of Blundy and Holland (1994). Equilibration temperatures of 742±50°C are based on twenty-one pairs of magnesiohornblende and andesine plagioclase compositions (Fig. 6b) at pressures between 0 and 2 kbar. Lower temperatures (645±50°C) were calculated from five pairs with oligoclase plagioclase compositions.

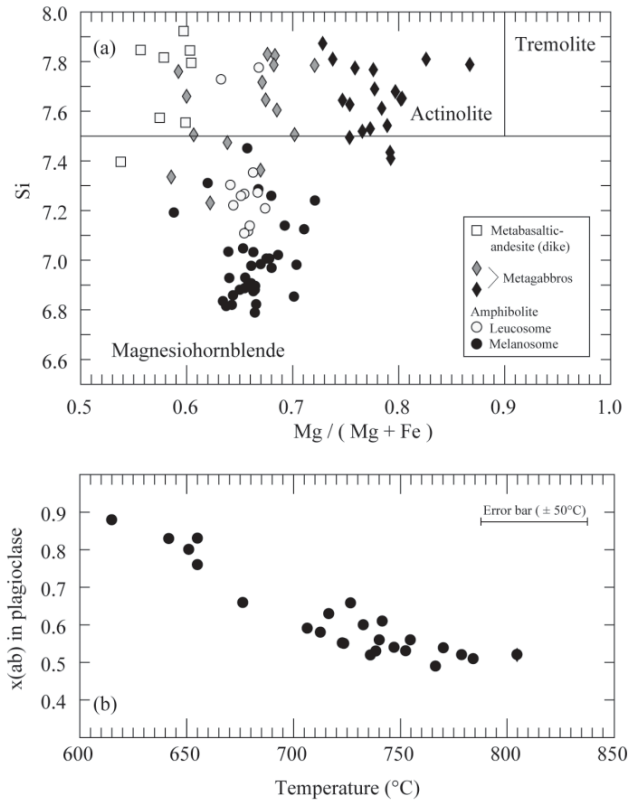

FIG. 6. **a-** Classification diagram of amphiboles (according to Leake *et al.*, 1997); **b-** Plot of mean temperature values calculated with the hornblende-plagioclase geothermometer of Blundy and Holland (1994). The mean temperature for different mineral pairs was calculated considering pressures of 0 and 2 kbar.

$^{40}Ar/^{39}Ar$ GEOCHRONOLOGY

Laser heating $^{40}Ar/^{39}Ar$ analyses of individual grains of metamorphic amphibole in rocks of the the Sarmiento Complex, were carried out in the Centro de Pesquisas Geocronológicas at the Universidade de São Paulo, Brazil. Detailed analytical procedures, including mineral separation, irradiation and mass spectrometric measurement procedures are presented by Vasconcelos *et al.* (2002). Although none of the analyses allow plateau ages to be calculated, some more or less concordant steps were used to calculate apparent 'forced plateau' ages. Results of $^{40}Ar/^{39}Ar$ analyses are listed in table 4.

The $^{40}Ar/^{39}Ar$ spectra of an individual amphibole grain separated from an amphibolite (sample ST0226B), displays little discordance except at one step in which a fall in the Ca/K ratio is related to an increase of the apparent age. The low Ca/K ratio of the analyzed grain (< 30) is akin to the ratios calculated for a low-silica magnesio-hornblende in an amphibolite (ST0226A) from the same outcrop. A forced plateau age of 172±5 Ma was calculated using four steps of the spectrum (Fig. 7a).

Two amphibole grains separated from a metagabbro (sample ST0229A), were analyzed. Both grains have Ca/K ratios between 50 and 100, which are similar to those for some actinolite grains in the same sample (magnesiohornblende in this sample have Ca/K ratios < 40). The spectrum of the first grain displays an old age in the lowest incremental heating step (Fig. 7b). A forced plateau age for this sample that was calculated from three steps yields an age of 151±12 Ma. The spectrum of the other grain shows less discordance and has a higher Ca/K ratio. A forced plateau age of 143±4 Ma for this sample was calculated using the first two steps (Fig. 7c).

The apparent age calculated for an amphibole grain of the amphibolite is about 20 Ma older than a zircon SHRIMP U-Pb crystallization age near 149 Ma for a plagiogranite. This age probably reflects excess ^{40}Ar in the amphibole grain that was incorporated either during amphibolite facies metamorphism and/or during the injection and crystallization of hornblende tonalitic melts. The ages of the actinolite in the metagabbro are concordant in part with the U-Pb zircon crystallization ages of the plagiogranite. Taking into consideration that perturbation of the K-Ar system in this rock is low (due to the lack of tonalitic segregations in the outcrop) and that the age calculated from the grain with the higher potassium content is more precise, an Early Cretaceous (*ca.* 140 Ma) metamorphic cooling age is suggested.

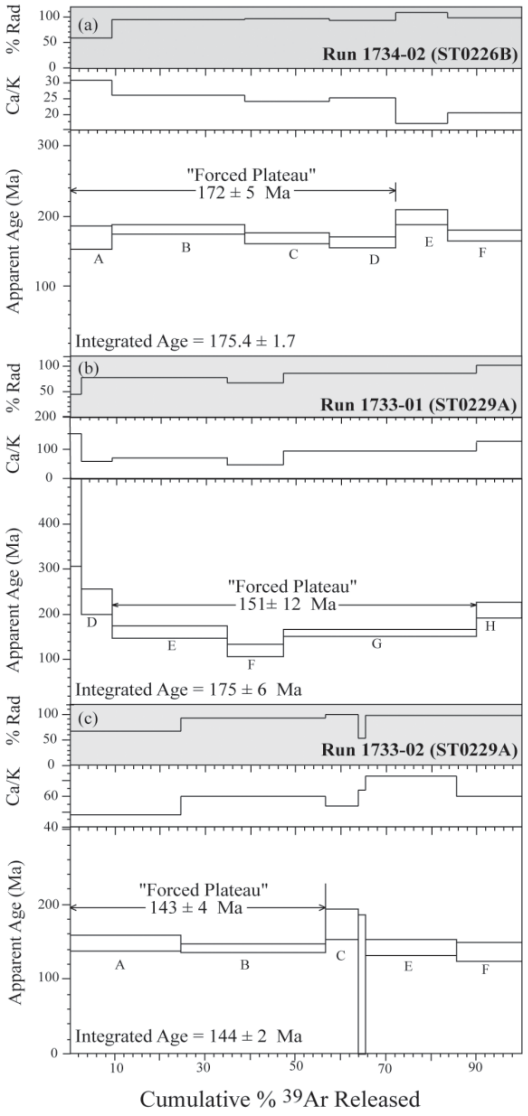

FIG. 7. $^{40}Ar/^{39}Ar$ gas release spectra for selected grains of metamorphic amphibole grains from a metagabbro and an amphibolite of the Sarmiento Complex.

TABLE 4. $^{40}Ar/^{39}Ar$ ANALYSES ON INDIVIDUAL AMPHIBOLE GRAINS FROM A METAGABBRO (ST0229A) AND AN AMPHIBOLITE (ST0226B).

Sample	Run ID#	Age (Ma)	± (Ma)	40/39	38/39	37/39	36/39	40*/39	% Rad
ST0226B	1734-01A	254.8	5.5	80.5	0.1	18.3	0.1	59.8	73.4
	1734-01B	192.1	3.1	48.6	0.1	15.4	0.0	44.3	90.2
	1734-01C	209.9	7.1	48.9	0.1	14.4	0.0	48.6	98.6
	1734-01D	209.3	13.9	56.1	0.1	15.6	0.0	48.5	85.5
	1734-01E	197.0	15.7	58.7	0.1	18.0	0.1	45.5	76.6
	1734-01F	187.2	4.5	51.2	0.1	14.6	0.0	43.1	83.4
	1734-01G	202.6	5.1	53.4	0.1	16.7	0.0	46.9	86.9
ST0226B	1734-02A	169.5	8.3	66.7	0.1	15.9	0.1	38.8	57.6
	1734-02B	181.0	3.1	43.4	0.1	13.4	0.0	41.6	95.0
	1734-02C	168.3	3.6	39.7	0.1	12.3	0.0	38.6	96.2
	1734-02D	162.6	3.7	40.2	0.1	12.9	0.0	37.2	91.7
	1734-02E	198.7	4.9	42.3	0.1	8.7	0.0	45.9	108.0
	1734-02F	172.0	3.8	40.3	0.1	10.5	0.0	39.4	97.1
ST0226B	1734-03A	270.5	11.9	84.1	0.1	11.1	0.1	63.8	75.3
	1734-03B	194.0	4.2	47.5	0.1	12.3	0.0	44.8	93.5
	1734-03C	178.9	3.1	40.9	0.1	12.1	0.0	41.1	99.6
	1734-03D	167.4	4.0	39.9	0.1	14.8	0.0	38.3	95.1
	1734-03E	240.5	12.6	49.3	0.0	14.9	0.0	56.2	112.9
	1734-03F	182.9	3.6	46.8	0.1	15.0	0.0	42.1	88.9
ST0229A	1733-01A	-1,381.5	1731.5	-8.0	0.6	0.0	0.7	-210.9	-
	1733-01B	0.0	2,5533.7	3,359.7	22.9	155.2	26.3	-4,891.2	-
	1733-01C	466.3	80.0	245.1	0.1	74.8	0.5	116.3	45.1
	1733-01D	227.4	14.0	67.2	0.0	28.0	0.1	53.0	77.3
	1733-01E	160.3	6.8	46.3	0.1	36.3	0.0	36.6	77.2
	1733-01F	120.3	6.5	39.8	0.1	24.6	0.1	27.2	67.3
	1733-01G	159.5	3.9	41.0	0.1	46.9	0.0	36.4	86.1
	1733-01H	209.6	9.0	46.2	0.1	62.6	0.0	48.6	100.8
ST0229A	1733-02A	148.5	5.2	49.6	0.0	24.6	0.1	33.8	67.1
	1733-02B	141.2	2.9	33.8	0.1	30.7	0.0	32.1	93.0
	1733-02C	172.8	10.1	38.8	0.1	27.4	0.0	39.6	100.2
	1733-02D	88.0	49.3	36.0	0.1	32.7	0.1	19.7	53.5
	1733-02E	142.7	5.3	32.3	0.1	37.3	0.0	32.5	98.1
	1733-02F	136.9	6.4	31.1	0.1	30.8	0.0	31.1	97.9

ISOTOPIC COMPOSITIONS

Sr and Nd isotopic analyses were performed in the Centro de Pesquisas Geocronológicas (Universidade de São Paulo). Rock samples for isotopic analysis consisted of 1-3 kg of material, which were crushed and split to 200g, and then powdered in a tungsten carbide mill. Rb and Sr contents were determined by X-ray fluorescence spectrometry. $^{87}Sr/^{86}Sr$ ratios were measured by thermal ionization mass-spectrometry, corrected for mass fractionation to $^{86}Sr/^{88}Sr=0.1194$ normalization. Sm and Nd (and other lanthanides) were chemically separated in HDEHP columns supported on teflon powder. The Sm and Nd concentrations were obtained by isotopic dilution using a mixed ^{149}Sm and ^{150}Nd tracer. The isotopic ratios were calculated relative to $^{146}Nd/^{144}Nd=0.7219$. All analyses of radiogenic isotopes were performed using a VG 354 Micromass spectrometer. At the time of the

analyses the following standard values were obtained: $^{87}Sr/^{86}Sr=0.71026\pm0.00002$ (2σ) for NBS-987 and $^{143}Nd/^{144}Nd=0.511847\pm0.00002$ (2σ) and 0.512662±0.000027 (2σ) values for La Jolla and BCR-1 respectively.

SHRIMP U-Pb geochronological determinations on zircons from felsic dikes of the Sarmiento Complex and metamorphosed tuffs of the Tobífera Formation show that mafic and felsic magmatism occurred between 152 and 147 Ma (Calderón *et al.*, in press). Age dependant isotopic ratios were calculated at 150 Ma for most samples with the exception of those collected from late (?) plutonic rocks and dikes in the Sarmiento Complex. For these rocks, we assumed an age of 140 Ma based on published radiometric ages (*e.g.*, Stern *et al.*, 1992; $^{40}Ar/^{39}Ar$ analyses in this study) and field relations. The sample with the lowest $^{147}Sm/^{144}Nd$ ratio (0.064; dolerite) shows the largest variation, one epsilon-neodynium unit (ε_{Nd}) when calculated either at 100 or at 150 Ma. Other samples show variations of around 0.2 epsilon units. Whole rock Sr and Nd isotopic data are listed in table 5 and isotopic relations are plotted in figure 8.

Metasedimentary rocks yielded $^{87}Sr/^{86}Sr$ initial ratios (Sr_{150}; calculated at 150 Ma) of 0.71757 (psammo-pelitic schist) and 0.72703 (pelitic schist) and correspondingly low initial ε_{Nd150} values of -4.4 and -9.1, respectively. Depleted mantle model ages (T_{DM}; after DePaolo *et al.,* 1991) are 1,322 and 1,660 Ma, respectively.

Mafic meta-igneous rocks in the Sarmiento Complex have relatively depleted isotopic compositions with ε_{Nd150} values ranging between +0.8 and +2.3 and T_{DM} between 624 and 706 Ma. The higher values of ε_{Nd150} (+2 and +2.3) correspond to the fine-grained dike of gabbro and the amphibolite. The pillow basalt yielded Sr_{150} of 0.70427 and ε_{Nd150} of +1.1. The plagiogranite showed a ε_{Nd150} value of +2.2.

Coarse and fine-grained granophyres in the mafic-felsic intrusive layer yielded more crustal-like ε_{Nd150} values ranging from -5.1 to -5.5 and T_{DM} model ages around 1,300 Ma. The massive dike of allanite-bearing dacite and of brecciated dacite in the mafic-felsic extrusive layer, have lower ε_{Nd150} values of -3.9 and -2.9, than the granophyres. A foliated metatuff in this layer yielded a ε_{Nd150} value of -5.1 that is indistinguishable from the values in the granophyres.

The hornblende dacite yielded a Sr_{140} of 0.704420 and a ε_{Nd140} of +0.9, which is similar to that

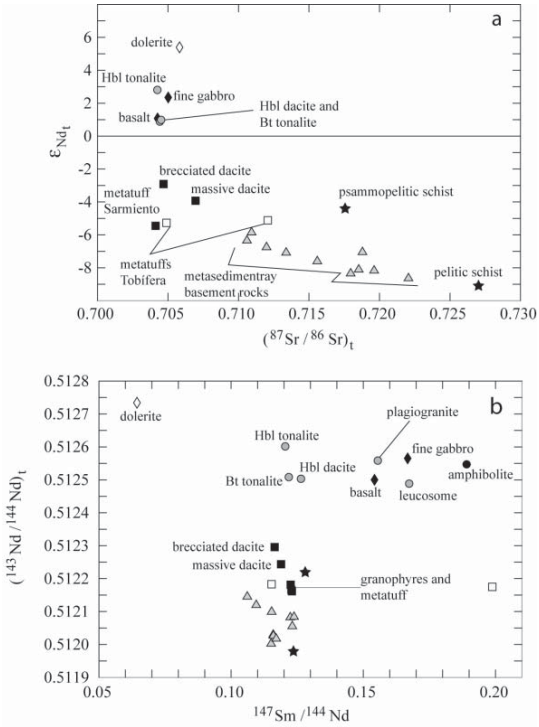

FIG. 8. **a-** Plot of the initial $^{87}Sr/^{86}Sr$ ratios *versus* the values of ε_{Ndt}; **b-** Plot of the $^{147}Sm/^{144}Nd$ ratio *versus* the initial $^{143}Nd/^{144}Nd$ ratio. Lithology of samples is indicated in the figure 2.

in the tonalitic leucosome in the amphibolite (+0.8). The hornblende tonalite yielded a Sr_{140} of 0.70425, a T_{DM} model age of 577 Ma and an ε_{Nd140} value of +2.8. Both rocks, which were collected from the mafic-felsic intrusive layer, have similar ratios to the metamorphosed mafic rocks. The biotite tonalite, in the southern tip of the mafic-felsic extrusive layer, has a higher Sr_{140} of 0.70451, lower ε_{Nd140} +1.0 and slightly older T_{DM} model age (724 Ma). The significantly more primitive igneous rock in the Sarmiento Complex is the dolerite collected from a dike in the mafic extrusive layer, which has a ε_{Nd140} of +5.4, a T_{DM} of 369 Ma and an initial $^{87}Sr/^{86}Sr$ ratio of 0.70583.

Metatuffs of the Tobífera Formation have crustal-like isotopic compositions with ε_{Nd150} varying between -5.1 and -5.4, T_{DM} model ages of 1,139 and 1,169 Ma and Sr_{150} of *ca.* 0.707 (average value). The sample with the highest Sr_{150} (0.7121) is the metatuff, which contains lithic fragments of metasedimentary rocks among its constituents.

TABLE 5. Nd AND Sr COMPOSITION FROM SAMPLES COLLECTED IN DIFFERENT LITHOSTRATIGRAPHIC UNITS IN THE VICINITIES OF THE CORDILLERA SARMIENTO.

Sample	Lithology	Age Ma	Sm ppm	Nd ppm	$^{147}Sm/^{144}Nd$	$^{143}Nd/^{144}Nd$	$(^{143}Nd/^{144}Nd)_t$	ε_{Ndt}	T_{DM} Ma	Rb ppm	Sr ppm	$^{87}Rb/^{86}Sr$	$^{87}Sr/^{86}Sr$	$(^{87}Sr/^{86}Sr)_t$
ST0306	Psammo-pelitic schist	150	2.71	12.78	0.1280	0.512345	0.512219	-4.4	1322	60.6	78.0	2.252	0.722369	0.717567
FO00101	Pelitic schist	150	6.58	32.21	0.1236	0.512100	0.511979	-9.1	1660	287.8	92.9	8.995	0.746210	0.727030
ST02-45B	Basalt	150	2.90	11.36	0.1542	0.512651	0.512500	1.1	774	6.9	20.9	0.959	0.70631	0.704265
ST0322B	Fine-grained gabbro (dike)	150	1.85	6.70	0.1668	0.512729	0.512565	2.3	659					0.705018
ST02-26BN	Melanosome (amphibolite)	150	1.12	3.58	0.1894	0.512732	0.512547	2.0	692					
ST02-26BL	Leucosome (amphibolite)	150	5.12	18.50	0.1673	0.512653	0.512489	0.8	796					
ST0322A	Plagiogranite	150	7.76	30.17	0.1555	0.5127112	0.512559	2.2	675					
ST0337	Hornblende dacite	140	1.86	8.91	0.1264	0.512619	0.512503	0.9	791	80.8	592.7	0.394	0.705204	0.704420
ST02-33A	Hornblende tonalite	140	4.15	20.85	0.1205	0.512712	0.512602	2.8	577	42.7	804.3	0.154	0.704553	0.704247
ST02-50	Biotite tonalite	140	4.44	22.01	0.1218	0.512620	0.512508	1.0	724	60.5	346.9	0.504	0.705518	0.704514
ST0329	Dolerite (dike)	140	0.86	8.04	0.0644	0.512793	0.512734	5.4	361					0.705826
ST02-32A	Granophyre	150	6.14	30.19	0.1230	0.512282	0.512161	-5.5	1309					
ST02-27	Granophyre	150	6.31	31.12	0.1225	0.512302	0.512181	-5.1	1280					
ST02-46	Masive dacite (dike)	150	5.45	27.70	0.1189	0.512360	0.512244	-3.9	1189	130.8	35.6	10.635	0.729634	0.706956
ST02-45A	Brecciated dacite	150	4.07	21.11	0.1165	0.512410	0.512296	-2.9	1109	145.4	46.3	9.103	0.724100	0.704689
ST02-03	Sheared felsic tuff	150	6.52	32.08	0.1228	0.512286	0.512166	-5.4	1304	74.5	78.0	2.766	0.710020	0.704122
ST02-51B	Sheared felsic tuff	150	2.27	6.91	0.1988	0.512370	0.512175	-5.3	1289	120.0	66.2	5.252	0.716090	0.704892
ST0249C	Lapilli crystal felsic tuff	150	2.93	15.34	0.1153	0.512296	0.512183	-5.1	1277	60.5	23.7	7.415	0.727890	0.712079
ST02-51C	Sheared felsic tuff	150								23.4	76.8	0.882	0.710089	0.708208
ST02-51G	Sheared felsic tuff	150								153.4	75.9	5.858	0.717435	0.704944
ST02-53	Sheared felsic tuff	150								61.2	32.2	5.510	0.716539	0.704791

DISCUSSION

The lithological, metamorphic and geochemical variations in the Sarmiento Complex have been considered to be like those recognized in diverse ophiolite complexes (Stern *et al.*, 1976; Stern, 1979; Saunders *et al.*, 1979; de Wit and Stern, 1981). The development of secondary phases without schistosity and the downward increase in metamorphic grade from zeolite to greenschist to amphibolite facies within a variable and short vertical sequence (1-3 km) have been associated with processes of seafloor hydrothermal metamorphism (Stern *et al.*, 1976). Greenschist facies dynamic metamorphism and the development of sheared belts in the Sarmiento Complex and Tobífera Formation, are probably associated with processes of ophiolite emplacement that are beyond the scope of this paper. Nevertheless, it is possible that some of the shearing was oceanic in setting.

MANTLE SOURCES AND MAFIC MAGMATISM

Geochemical data from metamorphosed mafic rocks of the Sarmiento Complex (Stern, 1979; Saunders *et al.*, 1979; Fildani and Hessler, 2005) put constraints on compositional features of the mantle source that produced the mafic magmas. The rare-earth-element (REE) patterns (mostly mafic lavas and dikes) show La_N/Lu_N ratios ranging between 1.6 and 3.3 after normalization to chondrites (according to Sun and Mcdonough, 1989; Fig. 9a). The lack of heavy REE depletion in the chondrite normalized patterns suggests partial melting processes in the upper mantle in the spinel- or plagioclase-lherzolite stability field (P < 15 GPa). Multi-element variation diagrams for metamorphosed mafic rocks after normalization to normal-mid-ocean-ridge-basalt (Sun and Mcdonough, 1989; Fig. 9b) display erratic and enriched values in large-ion- lithophile-elements (LILE), such as Rb, Ba and K compared to high-field-strength-element such as Nb and Ta. They also show more or less pronounced Nb-Ta and weak Ti negative anomalies. These compositional features are similar to those in continental and island arc basalts (Pearce, 1982) and suggest that the source of the mafic magmas was affected by processes related with a supra-subduction setting. A low degree of partial melting of the mantle sources seems to be needed. A sign of fluid- or melt-driven metasomatism in the mantle source is the low initial $^{143}Nd/^{144}Nd$ ratios in the metamorphosed mafic rocks that indicate a time-integrated enrichment of Nd relative to Sm in the mantle source.

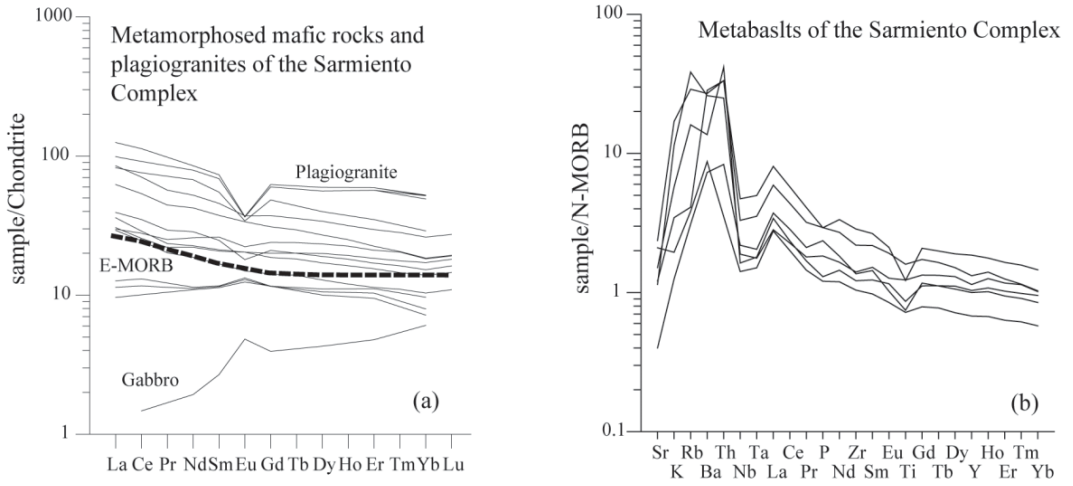

FIG. 9. **a-** Chondrite-normalized REE patterns of metamorphosed mafic rocks and plagiogranite of the Sarmiento Complex. Segmented line represents the E-MORB composition; **b-** Multi-element variation diagram normalized to N-MORB of metamorphosed mafic rocks. Geochemical data from Saunders *et al.* (1979), Stern (1979) and Fildani and Hessler (2005). Normalizing values are from Sun and McDonough (1989).

A primitive mantle source is required by the isotopic composition of the dolerite dike. Mineralogical similarities with the late or post-tectonic dolerite dikes in the metarhyolites of the Tobífera Formation (at Cordillera Riesco) suggest that these rocks belong to a younger episode of mafic magmatism in which mantle sources and tectonic conditions were different. These dolerite dikes could be related to the Cretaceous mafic magmatism of the Barros Arana Formation, which was derived from depleted subcontinental mantle sources (cf. Stern, 1991).

Tholeiitic fractional crystallization trends during mafic magmatism have been indicated by Stern (1979), supported in part by progressive variations in Mg-number of clinopyroxene (Fig. 4a). The titanium-rich clinopyroxene compositions in the metabasalt resemble those in alkaline rocks on clinopyroxene discrimination diagrams [(Ca+Na) *versus* Ti (not shown); Leterrier *et al.*, 1982]. Nevertheless, the high titanium content in this phase could be controlled by magma chemistry and fast cooling rate at the time of crystallization of basalts (cf. Tracy and Robinson, 1977). High titanium content in the clinopyroxene is consistent with an evolved composition of the basaltic magma (supported by the low Mg-number) and quenching processes are suggested by pillow structures and branching texture.

FELSIC MAGMATISM

The petrological meaning of the granophyre and dacite in the bimodal layers of the Sarmiento Complex is a key subject point. Whole rock chemical analyses and inherited components in zircon crystals from granophyres (dated at 147±10 Ma) have been taken as evidence of their derivation from melting of continental material bordering the mafic complexes into which the mafic magmas intruded (cf. Saunders *et al.*, 1979; de Wit and Stern, 1981; Stern *et al.*, 1992). Furthermore, Nd isotopic compositions of metamorphosed felsic rocks support the involvement of crustal components during magma genesis.

The plagiogranites, with SiO_2 contents between 66-75 wt%, relatively enriched and subparallel REE patterns as compared with the metabasalts, and showing Eu depletion (Fig. 9a), have been suggested to result from extreme fractional crystallization of mafic magmas (Stern, 1979). Nevertheless, diverse ophiolite studies have revealed that the roofs of axial magma chambers can be marked by polyphase magmatism, partial melting of amphibolites and intense interaction between hydrothermal fluids and rocks (*e.g.*, Gillis and Coogan, 2002 and references therein). Hornblende-plagioclase geothermometry (*ca.* 740±50°C) in an amphibolitic inclusion hosted in the hornblende tonalite indicates that disequilibrium partial melting (*e.g.,* T > 900°C at P = 0.2 GPa; cf. Koepke *et al.*, 2004) and melt segregation processes occurred in deeper portions of the ophiolite pseudostratigraphy. Therefore, the origin of plagiogranites, and probably of the small volume hornblende-bearing lithologies in the Sarmiento Complex could involve water-satured melts derived through anatexis of amphibolitized gabbros. A similar origin has been proposed for the generation of silicic differentiates in sea-floor spreading centers, such as plagiogranites in ophiolites (Gillis and Coogan, 2002) and silicic volcanic rocks in Iceland (Gunnarsson *et al.*, 1998).

THERMOCHEMICAL MODEL

The integration of energy, species and mass conservation into simulations of assimilation, and fractional crystallization processes in complex magmatic systems is possible with the energy-constrained assimilation fractional-crystallization (EC-AFC) model (Spera and Bohrson, 2001; Bohrson and Spera, 2001). This model follow the thermochemical evolution of an open-system magma body through solution of a system of coupled, non-linear ordinary differential equations that express conservation of energy, mass and species (trace elements and isotopes). The thermochemical approach used below considers two subsystems (for details see Spera and Bohrson, 2001; Bohrson and Spera, 2001): a homogeneous magma body of initial mass M_0 and a finite mass of surrounding country rocks. Solution of the EC-AFC provides values for the assimilant temperature (T_a), mass of melt within the magma body (M_m), mass of cumulates (M_c), mass of anatectic melt assimilated (M_a^*) and concentration of trace element and isotopic ratios in melt as a function of magma temperature (T_m). Input parameters include the equilibration temperature (T_{eq}), the initial temperature and isotopic composition of pristine magma (T_m^o and ε_m) and wall rock (T_a^o and ε_a), temperature-dependent trace element distribution coefficients (D_m and D_a), heats of transition for pristine melt and wall rock (Δ_m and Δh_a) and the isobaric specific heat capacity of pristine melt and

assimilant ($C_{p,m}$ and $C_{p,a}$). Melt-productivity functions [$f(T_m)$ and $f(T_a)$] exhibit non-linear sigmoidal forms in melt fraction *versus* temperature at fixed pressure and volatiles fugacity. Phase transition enthalpies and specific heat capacities are taken from the literature (Spera, 2000; Bohrson and Spera, 2001; Fowler *et al.*, 2004). The temperature dependence of the trace-element partition coefficient is estimated from literature. Because the Sm-Nd isotopic system seems to be unaffected by greenschist and amphibolite facies metamorphism (not the case for the Rb-Sr system; *e.g.,* DePaolo, 1988), solely the Nd isotopic composition of the studied rocks are considered in the following discussion.

The thermochemical model for the petrogenesis of the allanite-bearing granophyres and dacitic dikes in the bimodal layers (models 1 and 2) requires the choice of an appropriate Nd composition representative of the crustal assimilant at the time of the emplacement of mafic magmas. At the latitudes of the Sarmiento Complex, rifting in the Rocas Verdes basin probably began in the pre-Jurassic continental basement rocks of southwestern Gondwana. These rocks are represented in the studied area by the metasedimentary rocks of the Staines Complex. These psammopelitic and pelitic schists have ε_{Nd150} of -4.4 and -9.1, respectively. These are the most extreme isotopic values (Fig. 8) measured on Paleozoic metasedimentary rocks east of the South Patagonian batholith. Because the metasedimentary rocks of the Staines Complex share common petrographic features, structures and zircon detrital patterns, with metasedimentary rocks of the Eastern Andean Metamorphic Complex (cf. Hervé *et al.*, 2003), the correlation of both complexes is suggested. Consequently the average Nd isotopic composition of existing data (Augustsson, 2003; Calderón *et al.*, 2007) is considered representative of the composition of the crustal assimilant. The assumed average isotopic composition of the crustal assimilant used in the calculation is ε_{Nd} of -7.3. The composition of the fine-grained gabbro in the mafic-felsic intrusive layer is considered representative of the pristine mafic magmas. Selected results of the EC-AFC simulation are illustrative of a basaltic magma intruded at a liquidus temperature of 1200°C (T_m^o) into an upper crust with ambient temperatures of 300°C (T_a^o in model 1) and 400°C (T_a^o in model 2). These temperatures are within the range expected in a rift setting. The local liquidus and solidus temperatures of the pelitic crustal assimilant are T_s=715°C and T_s=900°C. The equilibration temperature T_{eq} is 870°C for both cases. Model 3 judges the thermal interaction between the mafic magmas and the host amphibolitic mafic crust in producing the plagiogranite. In model 3, the isotopic composition of the amphibolite is considered to be that of the mafic assimilant. All input parameters and comprehensive information are listed in table 6 and the models are shown by the lines labelled M1, M2, and M3 in figure 10.

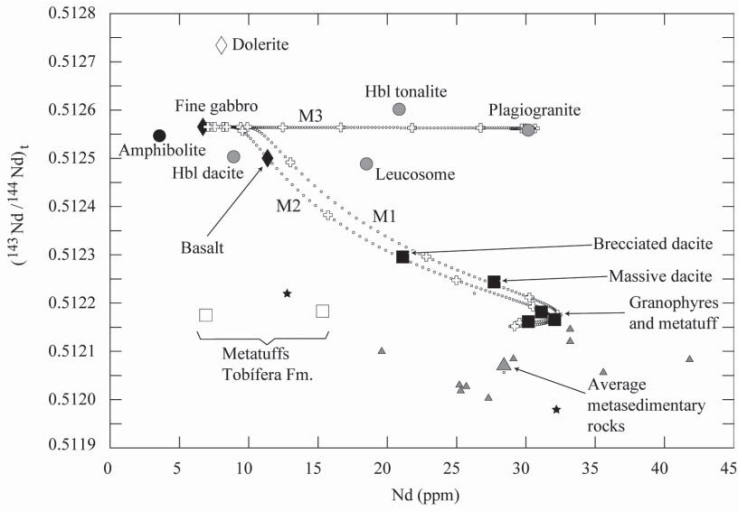

FIG. 10. Nd (ppm) *versus* $^{143}Nd/^{144}Nd$ results for EC-AFC models in bimodal meta-igneous rocks of the Sarmiento Complex. Dashed lines are EC-AFC model paths. The thermochemical models for the petrogenesis of the allanite-bearing granophyres and dacitic dikes (models 1 and 2; lines labelled M1 and M2 respectively) and plagiogranite (model 3; line labelled M3) are illustrated. See text and table 6 for more details.

TABLE 6. EC-AFC PARAMETERS, GRANOPHYRE AND DACITE (MODELS 1 AND 2) AND PLAGIOGRANITE (MODEL 3), SARMIENTO COMPLEX.

Thermal parameters	**Model 1**	**Model 2**	**Model 3**
Magma liquidus temperature (°C), $T_{l,m}$	1,200	1,200	1,200
Magma initial temperature (°C), $T_m°$	1,200	1,200	1,200
Assimilant liquidus temperature (°C), $T_{l,a}$	850	850	1,030
Assimilant initial temperature (°C), $T_a°$	300	400	700
Solidus temperature (°C), T_s	715	715	730
Equilibration temperature (°C), T_{eq}	870	870	795
Crystallization enthalpy (J/kg), Δh_{crys}	396,000	396,000	396,000
Isobaric specific heat of magma (J/kg per K), $C_{p,m}$	1,484	1,484	1,484
Fusion enthalpy (J/kg), Δh_{fus}	270,000	270,000	333,000
Isobaric specific heat of assimilant (J/kg per K), $C_{p,a}$	1,370	1,370	1,400
Compositional parameters (Nd)	**Model 1**	**Model 2**	**Model 3**
Magma initial conc. (ppm), Cm°	6.7	6.7	6.7
Magma isotope ratio, ε_m	0.512565	0.512565	0.512565
Magma trace element distribution coefficient, D_m	0.25	0.25	0.25
Assimilant initial conc. (ppm), $C_a°$	28.4	28.4	3.6
Assimilant isotope ratio, ε_a	0.512071	0.512071	0.512555
Assimilant trace element distribution coefficient, D_a	0.25	0.25	0.25
Enthalpy of trace element distribution coeffcient, ΔH_a	-9,000	-9,000	

Assimilant in models 1 and 2 is the average composition of metasedimenray rocks (pelite and psammopelite in composition) of the basement metamorphic rocks. Assimilant in model 3 is the amphibolite analyzed in this study. The composition of the fine-grained gabbro (dike) is considered for the pristine magma.

The good fit between the actual data and the models in figure 10 justifies using the calculated curves that are labeled M1 and M2 as tentative solutions to explain the isotopic variations seen in the mafic-felsic igneous layers of the Sarmiento Complex. As shown by Bohrson and Spera (2001), geochemical trends using the EC-AFC model display non-monotonic behaviours linked to energy conservation and partial melting of the country rock. After the mafic magma temperature decreases by 180°C the subhorizontal fractional crystallization trend is interrupted and gives rise to a steep mixing curve between the mafic magma and the radiogenic crustal rock (Fig. 10). A quantitative evaluation of the contamination of the basaltic magma by the crustal wall rocks indicates a Ma^*/Mc (mass of anatectic melt assimilated/ mass of cumulates) ratio of 0.04 (in model 2; T_a=745°C). Although small compositional differences between the basaltic lava and dike could be due to source heterogeneities, the model is in agreement with fractional crystallization being the main process involved in the evolution of mafic magmas.

The quantitative analyses of magma contamination in the granophyres indicate Ma^*/Mc ratios between 0.63-0.89 at T_m between 895-920°C and with T_a of 795-820°C. In the case of the dacites from the mafic-felsic extrusive layer, Ma^*/Mc ratios are lower (0.28-0.35), T_m are higher (975-945°C) and T_a are lower (770-780°C). The meta-tuffaceous rocks in the mafic-felsic extrusive layer show similar results to those for the granophyres. The differences in the degree of crustal assimilation among the metamorphosed felsic rocks could be related to different residence times for the silicic magmas in the magmatic reservoirs, controlled in part by the ease of eruption in response to the regional stress field.

The results for model 3 for the plagiogranite petrogenesis are consistent with the fractionation model of Stern (1979). They predict the 13% assimilation of the amphibolitic mafic crust (Ma^*/Mc ratio of 0.13).

TECTONO-MAGMATIC MODEL

The development of the Rocas Verdes basin probably involved periods of variable spreading rates that favored either the extrusion of large volumes of basaltic rocks or the emplacement and evolution of axial mafic magma chambers. The conceptual model for bimodal magmatism in the early tectonic evolution the Sarmiento Complex requires an early upper crustal magma chamber that formed by continuous basaltic injection from mantle reservoirs (Fig. 11). The accumulation of mafic magmas, which probably occurred after a period of rapid extension and voluminous submarine mafic volcanism, triggered crustal anatexis, segregation and accumulation of silicic melts with crustal isotopic compositions. The granophyres crystallized in the relatively 'quiet' tectonic zones, whereas the allanite-bearing dacitic dikes crystallized from magmas that travelled through remnant brittle deformed pathways along the rift axis.

A renewed pulse of extension and extrusion of the mafic magmas is represented by the dike complexes of fine-grained gabbro and basaltic flows in the mafic extrusive layer (Fig. 11). Subsequently, remnant gabbroic portions of the ophiolitic crust underwent hydrothermal metamorphism and anatexis during this episode of enhanced magmatic heat flux from the mantle. Even though there is lack of age control in the hornblende-bearing lithologies in the Sarmiento Complex, the above processes must be considered in the generation of the water-saturated magmas (hornblende-bearing intermediate igneous rocks) along axial magma chambers (Fig. 11).

A magmatic origin similar to that of the allanite-bearing granophyres and dacitic dikes of the Sarmiento Complex is suggested for the metatuffs of the Tobífera Formation, which also formed part of the seafloor of the Rocas Verdes basin. These tuffs share similar ε_{Nd150} values (of *ca.* -5) with the granophyres. Nevertheless, differences in the Nd and SiO_2 contents between the metatuffs (Nd between 6-16 ppm and SiO_2 of 78-81 wt%) and the granophyres (Nd of *ca.* 30 ppm and SiO_2 of 70-73 wt%) suggest that variable thermal regimes of magmatic reservoirs, caused by different rates of mafic magma recharge during magmatic chamber evolution, crustal heterogeneities, and other factors, exerted control over processes of assimilation and fractional crystallization. The periodic influx of mafic magmas and their interaction with the metapelites in the volcanic rifted continental crust may represent a first-order heat contribution for crustal anatexis and silicic magmatism during the early Rocas Verdes basin formation.

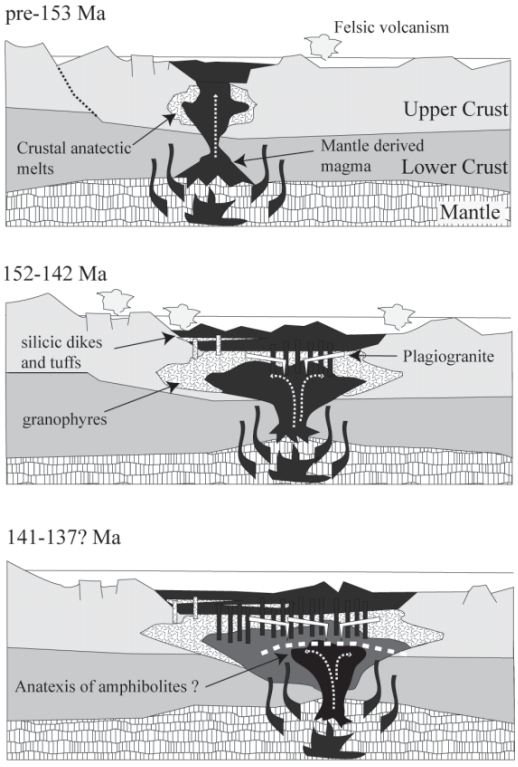

FIG. 11. Hypothetical and schematic model for the petrogenesis of mafic, felsic and intermediate igneous rocks in the Sarmiento Complex. The sketch figure (not to scale) shows the different lithologies considered in this study.

CONCLUSIONS

According to the discussions and available geochemical and isotopic data, the following points are worthy of note.

1. Metamorphosed mafic rocks and a plagiogranite from different layers in the ophiolite pseudostratigraphy of the Sarmiento Complex are char-

acterized by ε_{Nd150} values ranging between +1 and +2. Isotopic and trace element compositions suggest that mafic magmas were derived from an enriched mantle source, previously affected by metasomatism in a supra-subduction setting.

2. The progressive variation in Mg-number of the relict augitic pyroxene records the processes of fractional crystallization operating in the mafic magma chambers and along the magmatic/ structural pathways.

3. The felsic rocks in the bimodal layers of the Sarmiento Complex have crustal-like isotopic compositions. The ε_{Nd150} values of these granophyres range between -5 and -5.5, whereas those of the dacites are slightly higher (-3 to -4). These values exclude their derivation by fractional crystallization processes alone in the mafic magma chambers.

4. Quantitative thermochemical analyses indicate that the felsic rocks formed from magmas with mass of anatectic melt assimilated/mass of cumulates ratios (Ma^*/Mc) of 0.28-0.35 in the dacites and of 0.63-0.89 in the granophyres.

5. Model results for plagiogranite petrogenesis indicate that fractional crystallization is the dominant process, but also predict the assimilation of amphibolitic mafic crust by 13% (Ma^*/Mc of 0.13).

ACKNOWLEDGEMENTS

This study was financially supported by the Conicyt grant and the BAPRTD (M.C), Fondecyt grants 1010412 and 1050431 (F.H.) and Conicyt-BMBF grant to F.H. and H.-J. M. The Álvarez-McCloud family is acknowledged for their logistical and friendly support during the fieldwork in the remote sampling areas. We would like to thank A. Onoe, L. Petronilho, S. de Souza, H. Sonoki, I. Sonoki and V. Loios of the Centro de Pesquisas Geocronológicas (Universidade de São Paulo, Brazil) who helped with the acquiring and processing of the isotopic and geochronological data. T. Theye is acknowledged for his guidance during the work with the electron microprobe. We thank S. Kay, C. Stern, E. Moores and P. Thy for their constructive reviews.

REFERENCES

Allen, R.B. 1982. Geología de la Cordillera Sarmiento, Andes Patagónicos, entre los 51°00' y 52°15' Lat. S, Magallanes, Chile. Servicio Nacional de Geología y Minería, Boletín 38: 46 p.

Annen, C.; Sparks, R.S.J. 2002. Effects of repetitive emplacement of basaltic intrusions on thermal evolution and melt generation in the crust. Earth and Planetary Science Letters 203: 937-955.

Augustsson, C. 2003. Provenance of Late Palaeozoic sediments in the southern Patagonian Andes: age estimates, sources, and depositional setting. Dissertation, Westfälische Wilhelms-Universität Münster: 94 p.

Augustsson, C.; Münker, C.; Bahlburg, H.; Fanning, C.M. 2006. Provenance of late Palaeozoic metasediments of the SW South American Gondwana margin: a combined U-Pb and Hf-isotope study of single detrital zircons. Journal of the Geological Society, London, 163: 983-995.

Blundy, J.D.; Holland, T.J.B. 1994. Calcic amphibole equilibria and a new amphibole-plagioclase geothermometer. Contributions to Mineralogy and Petrology 104: 208-224.

Bohrson, W.A.; Spera, F.J. 2001. Energy-constrained open-system magmatic processes II: application of energy-constrained assimilation-fractional crystallisation (EC-AFC) model to magmatic systems. Journal of Petrology 42: 1019-1041

Bruhn, R.L.; Stern, C.R.; de Wit, M.J. 1978. Field and geochemical data bearing on the development of a Mesozoic volcano-tectonic rift zone and back-arc basin in southernmost South America. Earth and Planetary Science Letters 41: 32-46.

Calderón, M. 2005. Metamorfismo de alta temperatura y baja presión en rocas del basamento metamórfico en Puerto Edén, Magallanes, Chile. M.Sc. Thesis (Inédito), Universidad de Chile: 103 p.

Calderón, M. 2006. Petrogenesis and tectonic evolution of Late Jurassic bimodal magmatic suites (Sarmiento Complex) and migmatites (Puerto Edén Igneous Metamorphic Complex) in the southern Patagonian Andes, Chile. Ph.D. Thesis (Unpublished), Universidad de Chile: 170 p.

Calderón, M.; Galaz, G.; Tascón, G.; Ramírez, C.; Luca,

R.; Massonne, H-J.; Brandelik, A.; Hervé, F. 2005. Metamorphic P-T constraints for non-coaxial ductile flow of Jurassic pyroclastic deposits: key evidence for the closure of the Rocas Verdes basin in southern Chile. *In* International Symposium on Andean Geodynamics, No. 6, extended abstracts: 138-141. Barcelona

Calderón, M.; Hervé, F.; Massonne, H.-J.; Tassinari, C.G.; Pankhurst, R.J.; Godoy E.; Theye, T. 2007. Petrogenesis of the Puerto Edén Igneous and Metamorphic Complex, Magallanes, Chile: Late Jurassic syn-deformational anatexis of metapelites and granitoid magma genesis. Lithos 93:17-38.

Calderón, M.; Fildani, A; Hervé, F; Fanning, C.M.; Weislogel, A.; Cordani, U. In press. Late Jurassic bimodal magmatism in the northern seafloor remnant of the Rocas Verdes basin, southern Patagonian Andes. Journal of the Geological Society, London.

Dalziel, I.W.D. 1981. Back-arc extension in the southern Andes: A review and critical reappraisal: Royal Society of London Philosophical Transactions, series A 300: 319-335.

Dalziel, I.W.D.; de Wit, M.J.; Palmer, F. 1974. Fossil marginal basin in the southern Andes. Nature 250: 291-294. London.

de Wit, M.J.; Stern, C.R. 1981. Variation in the degree of crustal extension during formation of a back-arc basin: Tectonophysics 72: 229-260

DePaolo, D.J. 1988. Neodymium Isotope Geochemistry, An Introduction. Springer-Verlag: 187 p.

DePaolo, D.J.; Linn, A.M.; Schubert, G. 1991. The continental crustal age distribution; methods of determining mantle separation ages from Sm-Nd isotopic data and application to the Southwestern United States. Journal of Geophysical Research B96: 2071-2088.

Faúndez, V.; Hervé, F.; Lacassie, J.P. 2002. Provenance and depositional setting of pre-Late Jurassic turbidite complexes in Patagonia, Chile. New Zealand Journal of Geology and Geophysics 45: 411-425.

Fildani, A.; Cope, T.D.; Graham, S.A.; Wooden, J.L. 2003. Initiation of the Magallanes foreland basin: Timing of the southernmost Patagonian Andes orogeny revised by detrital zircon provenance analysis. Geology 31: 1081-1084.

Fildani, A.; Hessler, A.M. 2005. Stratigraphic record across a retroarc basin inversion: Rocas Verdes-Magallanes basin, Patagonian Andes, Chile. Geological Society of America Bulletin 117: 1596-1614.

Forsythe, R.; Allen, R.B. 1980. The basement rocks of Península Staines, Región XII, Province of Última Esperanza, Chile. Revista Geológica de Chile 10: 3-15.

Forsythe, R.; Mpodozis, C. 1983. Geología del basamento pre-Jurásico Superior en el archipiélago Madre de Dios, Magallanes, Chile. Servicio Nacional de Geología y Minería, Boletín 39: 63 p.

Fowler, S.J.; Bohrson, W.A.; Spera, F.J. 2004. Magmatic evolution of the Skye igneous centre, western Scotland: modelling of assimilation, recharge and fractional crystallization. Journal of Petrology 45: 2481-2505.

Fuenzalida, R.; Covacevich, V. 1988. Volcanismo y bioestratigrafía del Jurásico y Cretácico Inferior en la Cordillera Patagónica, Región de Magallanes, Chile. *In* Congreso Geológico Chileno, No. 5, Actas 3: H159-H183.

Galaz, G.; Hervé, F.; Calderón M. 2005. Metamorfismo y deformación de la Formación Tobífera en la Cordillera Riesco, Región de Magallanes, Chile. Revista de la Asociación Geológica Argentina 60 (4): 762-774.

Gillis, K.M.; Coogan, L.A. 2002. Anatectic migmatites from the roof of an ocean ridge magma chamber. Journal of Petrology 43: 2075-2095.

Grunder, A.L. 1995. Material and thermal roles of basalt in crustal magmatism: case study from eastern Nevada. Geology 23: 952-956.

Gunnarsson, B.; Marsh, B.D.; Taylor Jr., H.P. 1998. Generation of Islandic rhyolites: silicic lavas from the Torfajokull central volcano. Journal of Volcanology and Geothermal Research 83: 1-45.

Hervé, F.; Aguirre, L.; Godoy, E.; Massonne, H-J.; Morata, D.; Pankhurst, R.J.; Ramírez, E.; Sepúlveda, V.; Willner, A. 1998. Nuevos antecedentes acerca de la edad y las condiciones P-T de los complejos metamórficos en Aysén, Chile. *In* Congreso Latinoamericano de Geología, No. 10 y Congreso Nacional de Geología Económica, No. 6, Actas 2: 134-137. Buenos Aires, Argentina.

Hervé, F.; Fanning, C.M.; Pankhurst, R.J. 2003. Detrital zircon age patterns and provenance of the metamorphic complexes of southern Chile. Journal of South American Earth Sciences 16: 107-123.

Hervé, F.; Massonne, H-J.; Calderón, M.; Theye, T. 2004. Metamorphic P-T conditions of rhyolites in the Magallanes fold and thrust belt, Patagonian Andes. Bollettino di Geofisica teorica ed applicata, International Symposium on the Geology and Geophysics of the Southermost Andes, the Scotia Arc and the Antartic Peninsula, 45, Extended Abstracts: 15-18.

Hervé, F.; Pankhurst, R.J.; Fanning, C.M.; Calderón, M.; Yaxley, G.M. 2007. The South Patagonian batholith: 150 my of granite magmatism on a plate margin. doi:10.1016/j.lithos.2007.01.007.

Huppert, H.E.; Sparks, R.J.S. 1988. The generation of granitic magma by intrusion of basalt into continental crust. Journal of Petrology 29: 1-19.

Katz, H.R. 1964. Some new concepts on geosynclinal development and mountain building at the southern end of South America. *In* International Geological Congress, No. 22, Proceedings 4: 242-255. New Delhi, India.

Koepke, J.; Feig, S.T.; Snow, J.; Freise, M. 2004. Petrogenesis of oceanic plagiogranites by partial melting of gabbros: an experimental study. Contribution to Mineralogy and Petrology 146: 414-432

Lacassie, J.P.; Hervé, F.; Roser, B. 2006. Sedimentary provenance study of the post-Early Permian to pre-Early Cretaceous metasedimentary Duque de York Complex, Chile. Revista Geológica de Chile 33 (2): 199-219.

Leake, B.E.; Woolley, A.R.; Arps, C.E.S.; Birch, W.D.; Gilbert, M.C.; Grice, J.D.; Hawthorne, C.; Kato, A.; Kisch, H.J.; Krivovichev, V.G.; Linthout, K.; Laird, J.; Mandarino, J.A.; Maresch, W.V.; Nickel, E.H.; Rock, N.M.S.; Schumacher, J.C.; Smith, D.C.; Stephenson, C.N.; Ungaretti, L.; Whittaker, E.J.W.; Youzhi, G. 1997. Nomenclature of amphiboles: report of the subcommittee on amphiboles of the International Mineralogical Association, Commission on new minerals and mineral names. American Mineralogist 82:1019-1037.

Leterrier, J.; Maury, R.C.; Thonon, P.; Girard, D.; Marchal, M. 1982. Clinopyroxene composition as a method of identification of the magmatic affinities of paleo-volcanic series. Earth and Planetary Science Letters 59: 139-154.

Milord, I.; Sawyer, E.W.; Brown, M. 2001. Formation of diatexite migmatite and granite magma during anatexis of semi-pelitic metasedimentary rocks: an example from St. Malo, France. Journal of Petrology 42: 487-505.

Olivares, B.; Cembrano, J.; Hervé, F.; López, G.; Prior, D. 2003. Análisis estructural de rocas de una zona de cizalle dúctil en Isla Diego de Almagro, sur de Chile. Revista Geológica de Chile 30 (1): 39-52.

Pankhurst, R.J.; Rapela, C.W. 1995. Production of Jurassic rhyolite by anatexis of the lower crust of Patagonia. Earth and Planetary Science Letters 134: 23-36.

Pankhurst, R.J.; Tiley, T.R.; Fanning, C.M.; Kelley, S.P. 2000. Episodic silicic volcanism in Patagonia and Antarctic Peninsula: Chronology of magmatism associated with the break-up of Gondwana. Journal of Petrology 41: 605-625.

Patiño Douce, A.E. 1995. Experimental generation of hybrid silicic melts by reaction of high-Al basalt with metamorphic rocks. Journal of Geophysical Research, 100, B8: 15623-15639.

Patiño Douce, A.E.; Beard, J.S. 1995. Dehydration-melting of biotite gneiss and quartz amphibolite from 3 to 15 kbar. Journal of Petrology 36: 707-738.

Petford, N.; Gallagher, K. 2001. Partial melting of mafic (amphibolitic) lower crust by periodic influx of basaltic magma. Earth and Planetary Earth Science Letters 193: 483-499.

Pearce, J.A. 1982. Trace element characteristics of lavas from destructive plate boundaries, *In* Andesite: Orogenic Andesites and Related Rocks (Thorpe, R.S.; editor). Chichester Wiley: 525-548.

Rapp, R.P.; Watson, E.B. 1995. Dehydration melting of metabasalt at 8-32 kbar: implications for continental growth and crust-mantle recycling. Journal of Petrology 36: 891-931

Saunders, A.D.; Tarney, J.; Stern, C.R.; Dalziel, I.W.D. 1979. Geochemistry of Mesozoic marginal basin floor igneous rocks from southern Chile. Geological Society Bulletin of America 90: 237-258.

Spera, F.J. 2000. Physical properties of magmas. *In* Encyclopedia of Volcanoes (Sigurdsson, H.; editor), Academic Press: 171-190. New York.

Spera, F.J.; Bohrson, W.A. 2001. Energy-constrained open-system magmatic processes I: general model and energy-constrained assimilation-fractional crystallisation (EC-AFC) formulation. Journal of Petrology 42: 999-1018.

Stern, C.R. 1979. Open and closed system igneous fractionation within two chilean ophiolites and the tectonic implications. Contribution to Mineralogy and Petrology 68: 243-258.

Stern, C.R. 1991. Isotopic composition of Late Jurassic and Early Cretaceous mafic igneous rocks from the southernmost Andes: implications for sub-Andean mantle. Revista Geológica de Chile 18: 15-23.

Stern, C.R.; de Wit, M.J. 2003. Rocas Verdes ophiolites, southernmost South America: remnants of progressive stages of development on oceanic-type crust in a continental margin back-arc basin. *In* Ophiolites in Earth History (Dilek, Y.; Robinson, P.T.; editors), Geological Society, London, Special Publications 218: 1-19.

Stern, C.R.; de Wit, M.J.; Lawrence, J.R. 1976. Igneous and metamorphic processes associated with the formation of Chilean ophiolites and their implications for ocean floor metamorphism, seismic layering, and magnetism. Journal of Geophysical Research 81, 23: 4370-4380.

Stern, C.R.; Mukasa, S.B.; Fuenzalida, R. 1992. Age and petrogenesis of the Sarmiento ophiolite complex of southern Chile. Journal of South American Earth Sciences 6: 97-104.

Suárez, M.; Pettigrew, T.H. 1976. An Upper Mesozoic island-arc-back-arc system in the southern Andes and South Georgia. Geological Magazine 113: 305-328.

Sun, S.; McDonough, W.F. 1989. Chemical and isotopic systematics of oceanic basalts: implications for mantle composition and processes. *In* Magmatism in the ocean basins (Saunders, A.D.; Norris, M.J.; editors), Geological Society, London, Special Publications 42: 313-345.

Thomson, S.N.; Hervé, F. 2002. New time constraints for the age of metamorphism at the ancestral Pacific Gondwana margin of southern Chile (42-52°S). Revista Geológica de Chile 29 (2): 255-271.

Tracy, R.J.; Robinson, P. 1977. Zoned titanium augite in alkali olivine basalt from Tahiti and the nature of titanium substitutions in augite. American Mineralogist 62: 634-645.

Vasconcelos, P.; Onoe, A.; Kawashita, K.; Soares, A.; Texeira, W. 2002. $^{40}Ar/^{39}Ar$ geochronology at the

Instituto de Geociências, USP: instrumentation, analytical procedures, and calibration. Anais da Academia Brasileira de Ciências 74 (2): 297-342. Río de Janeiro.

Watters, W.A. 1964. Geological work at Puerto Edén, Wellington island, southern Chile. Transactions of the Royal Society of New Zealand, Geology 2 (11): 155-168.

Willner, A.P.; Hervé, F.; Thomson, S.N.; Massonne, H-J. 2004. Converging P-T paths of Mesozoic HP-LT metamorphic units (Diego de Almagro Island, Southern Chile): evidence for juxtaposition during late shortening of an active continental margin. Mineralogy and Petrology 81: 43-84.

Wilson, T.J. 1991. Transition from back-arc to foreland basin development in southernmost Andes: Stratigraphic record from the Ultima Esperanza District, Chile. Geological Society of America Bulletin 103: 98-111.

Wolf, M.B.; Wyllie, P.J. 1994. Dehydration-melting of amphibolite at 10 kbar: the effects of temperature and time. Contribution to Mineralogy and Petrology 115: 369-383

Manuscript received: September 14, 2006; accepted: April 2, 2007.